

Stochastic parareal: an application of probabilistic methods to time-parallelisation

Kamran Pentland^{*1}, Massimiliano Tamborrino², D. Samaddar³, and L. C. Appel³

¹*Mathematics Institute, University of Warwick, Coventry, C4 7AL, United Kingdom*

²*Department of Statistics, University of Warwick, Coventry, CV4 7AL, United Kingdom*

³*Culham Centre for Fusion Energy, Culham Science Centre, Abingdon, Oxfordshire, OX14 3DB, United Kingdom*

June 29, 2021

Abstract

Parareal is a well-studied algorithm for numerically integrating systems of time-dependent differential equations by parallelising the temporal domain. Given approximate initial values at each temporal sub-interval, the algorithm locates a solution in a fixed number of iterations using a predictor-corrector, stopping once a tolerance is met. This iterative process combines solutions located by inexpensive (coarse resolution) and expensive (fine resolution) numerical integrators. In this paper, we introduce a *stochastic parareal* algorithm with the aim of accelerating the convergence of the deterministic parareal algorithm. Instead of providing the predictor-corrector with a deterministically located set of initial values, the stochastic algorithm samples initial values from dynamically varying probability distributions in each temporal sub-interval. All samples are then propagated by the numerical method in parallel. The initial values yielding the most continuous (smoothest) trajectory across consecutive sub-intervals are chosen as the new, more accurate, set of initial values. These values are fed into the predictor-corrector, converging in fewer iterations than the deterministic algorithm with a given probability. The performance of the stochastic algorithm, implemented using various probability distributions, is illustrated on systems of ordinary differential equations. When the number of sampled initial values is large enough, we show that stochastic parareal converges almost certainly in fewer iterations than the deterministic algorithm while maintaining solution accuracy. Additionally, it is shown that the expected value of the convergence rate decreases with increasing numbers of samples.

1 Introduction

In its most basic form, parallel computing is the process by which an algorithm is partitioned into a number of sub-problems that can be solved simultaneously without prior knowledge of each other. More widespread parallelism is becoming increasingly necessary in many different fields to reduce the computational burden, and thus overcome the physical limitations (i.e. space, power usage, clock speeds, cooling, and financial costs) arising on machine hardware. Complex models in science often involve solving large systems of ordinary or partial differential equations (ODEs or PDEs) which, in the case of

^{*}Corresponding author: kamran.pentland@warwick.ac.uk

spatio-temporal PDEs, can be parallelised using existing domain decomposition methods. We refer to [1] for an overview. Although very efficient for high dimensional systems, these methods are reaching scale-up limits, and wallclock speeds often bottleneck due to the temporal integration. For instance, modern algorithms used to simulate Edge Localised Modes in turbulent fusion plasmas can take anywhere between 100-200 days to integrate over a time interval of one second [2].

These sequential bottlenecks in time have motivated the research and development of time-parallel integration methods for systems of ODEs and PDEs over the last 55 years or so (see [3, 4, 5] for reviews). These methods provide a way to integrate initial value problems (IVPs) over long time intervals where solutions would be unobtainable using existing sequential algorithms. One approach to integrate in a non-sequential manner, similar to spatial parallelisation, is to discretise the time interval into N sub-intervals upon which N sub-problems are solved in parallel using existing numerical techniques. The solution at a given time step, however, depends upon the solution at the previous step(s). This creates a problem prior to the parallel integration as $N - 1$ of the N initial values (from which to begin integration in each sub-interval) are unknown *a priori*. Existing algorithms that attempt to locate these $N - 1$ initial values by direct or iterative means have been collectively referred to as multiple shooting methods [6, 7, 8, 9, 10].

Our focus is on one multiple shooting method in particular: the parareal algorithm [8]. This algorithm uses a combination of coarse and fine grained (in time) numerical integrators to provide parallel speed-up, and has been tested successfully on problems ranging from molecular [11] and fluid dynamics [12, 13, 14], to stochastic differential equations [15, 16] and fusion plasma simulations [2, 17]. The popularity of parareal is due to its relatively straightforward implementation and demonstrable effectiveness in speeding up the integration of IVPs. The algorithm iteratively locates a numerical solution at each sub-interval using a predictor-corrector scheme, derived by discretising the Newton-Raphson method. The algorithm stops once a tolerance is met with convergence guaranteed under certain mathematical conditions - more detail on the algorithm is provided in section 2. Much work has gone into analysing the numerical convergence of this method [18, 19, 20, 21], combining it with spatial decomposition techniques [22], and developing variants that utilise idle processors [23] and adaptive time-stepping [24]. However, given fixed fine and coarse integrators, the method itself is strictly deterministic and little work has gone into trying to reduce the number of iterations $k_d \in \{1, \dots, N\}$ that parareal takes to solve a particular IVP. Our primary focus is on k_d and henceforth we refer to it as the ‘convergence rate’. In scenarios where parareal struggles to converge in $k_d \ll N$ iterations, reducing k_d by even a few iterations, say to $k_s < k_d$, can lead to parallel efficiency gains (roughly a factor k_d/k_s), enabling faster numerical integration.

The purpose of this work is to extend the parareal algorithm using probabilistic methods to converge in fewer than k_d iterations for a given system of ODEs. To achieve this, we introduce a *stochastic* parareal algorithm. Instead of integrating forward in time from a single initial value (given by the predictor-corrector) in each sub-interval, a pre-specified probability distribution (see sampling rules in section 3.3) is used to generate M candidate initial values that are *simultaneously* integrated forward in time in parallel. At each sub-interval, one optimal initial value (from the M samples) is selected sequentially such that the most continuous trajectory is chosen across consecutive sub-intervals. These initial values are then fed directly into the predictor-corrector - the idea being that this stochastically generated set of values provides a better guess to the solution than those found purely deterministically. For example, suppose running the predictor-corrector with initial values $\mathbf{x}^{(0)}$ yields convergence in k_d iterations, generating the sequence of solutions $\{\mathbf{x}^{(0)}, \mathbf{x}^{(1)}, \dots, \mathbf{x}^{(k_d)}\}$. Instead of starting with $\mathbf{x}^{(0)}$, suppose we sample initial values from a probability distribution and choose some “better” starting point which is close to, say, $\mathbf{x}^{(i)}$ for some $i \in \{1, \dots, k_d - 1\}$. Then the sequence generated by the predictor-corrector would instead be approximately $\{\mathbf{x}^{(i)}, \mathbf{x}^{(i+1)}, \dots, \mathbf{x}^{(k_d)}\}$, converging in $k_d - i$ iterations. Therefore, given a fixed number of samples M , the

stochastic parareal algorithm will converge in fewer than k_d iterations with some non-zero probability.

This idea of propagating multiple initial values in each sub-interval in parallel is not new. In the first major work proposing the time-parallel integration of IVPs, Nievergelt [9] discussed choosing M initial values deterministically. The method for determining the solution from this ensemble of trajectories was, however, to combine two of the M samples in each sub-interval using an interpolation coefficient determined from the preceding sub-interval. Whilst an excellent first incursion into the field, this direct method suffered from interpolation errors for nonlinear problems and questions remained on how to efficiently scale this up to systems of ODEs. We generalise the original idea of Nievergelt by combining it with the parareal algorithm, generating the M initial values at each sub-interval using probability distributions based on information known about the solutions at the current iteration.

The paper is organised as follows. In [section 2](#) we detail the parareal algorithm and its properties from a multiple shooting viewpoint, including a known modification that will enable us to extend the algorithm to incorporate stochastic sampling. In [section 3](#) we introduce the stochastic parareal algorithm. Following an explanation of its key features, we elucidate how a variety of different sampling rules can be flexibly interchanged in order to carry out the stochastic sampling. In [section 4](#) we conduct numerical experiments to illustrate the performance of stochastic parareal against its deterministic counterpart using the different sampling rules. Detailed findings are presented for three well-known systems of one, two, and three ODEs with two additional examples given in the Appendix. We show that for large enough M , stochastic parareal betters the convergence rate of the deterministic algorithm with probability approaching one and generates stochastic solutions that are accurate with respect to the standard algorithm. For systems of ODEs, it is shown that performance is improved by generating correlated samples, as opposed to uncorrelated. Finally in [section 5](#), conclusions are drawn and avenues for future research are discussed.

2 The parareal algorithm

Following previously outlined descriptions of the parareal algorithm [20, 8], henceforth referred to as ‘parareal’ or \mathcal{P} , consider a system of $d \in \mathbb{N}$ ODEs

$$\frac{d\mathbf{u}}{dt} = \mathbf{f}(\mathbf{u}(t), t) \quad \text{on } t \in [T_0, T_N], \quad \text{with } \mathbf{u}(T_0) = \mathbf{u}^0, \quad (1)$$

where $\mathbf{f} : \mathbb{R}^d \times [T_0, T_N] \rightarrow \mathbb{R}^d$ is a smooth multivariate (possibly nonlinear) function, $\mathbf{u} : [T_0, T_N] \rightarrow \mathbb{R}^d$ the time-dependent vector solution, and $\mathbf{u}^0 \in \mathbb{R}^d$ the initial values at T_0 . Decompose the time domain into N sub-intervals such that $[T_0, T_N] = [T_0, T_1] \cup \dots \cup [T_{N-1}, T_N]$, with each sub-interval taking fixed length $\Delta T := T_n - T_{n-1}$ for $n = 1, \dots, N$ (see [Figure 1](#) for a schematic).



Figure 1: Schematic of the time domain decomposition. Three levels of temporal discretisation are shown: sub-intervals (size ΔT), coarse intervals (size δT), and fine intervals (size δt). Note how the discretisations align with one another and that $\delta t \ll \delta T \leq \Delta T$ in our implementation.

Having partitioned the time domain, N smaller sub-problems

$$\frac{d\mathbf{u}_n}{dt} = \mathbf{f}(\mathbf{u}_n(t | \mathbf{U}_n), t) \quad \text{on } t \in [T_n, T_{n+1}], \quad \text{with } \mathbf{u}_n(T_n) = \mathbf{U}_n, \quad (2)$$

for $n = 0, \dots, N-1$ can theoretically be solved in parallel on N processors, henceforth denoted P_1, \dots, P_N . Each solution $\mathbf{u}_n(t | \mathbf{U}_n)$ is defined over $[T_n, T_{n+1}]$ given the initial values $\mathbf{U}_n \in \mathbb{R}^d$ at $t = T_n$. Note however that only the initial value $\mathbf{U}_0 = \mathbf{u}_0(T_0) = \mathbf{u}^0$ is known, whereas the rest (\mathbf{U}_n for $n \geq 1$) need to be determined before (2) can be solved in parallel. These initial values must satisfy the continuity conditions

$$\mathbf{U}_0 = \mathbf{u}^0 \quad \text{and} \quad \mathbf{U}_n = \mathbf{u}_{n-1}(T_n | \mathbf{U}_{n-1}) \quad \text{for } n = 1, \dots, N, \quad (3)$$

a (possibly nonlinear) system of $N+1$ equations that ensure solutions match at each $T_n \forall n \geq 1$. System (3) is solved for \mathbf{U}_n using the Newton-Raphson method to form the iterative system

$$\mathbf{U}_0^{k+1} = \mathbf{u}^0, \quad (4a)$$

$$\mathbf{U}_n^{k+1} = \mathbf{u}_{n-1}(T_n | \mathbf{U}_{n-1}^k) + \frac{\partial \mathbf{u}_{n-1}}{\partial \mathbf{U}_{n-1}}(T_n | \mathbf{U}_{n-1}^k) [\mathbf{U}_{n-1}^{k+1} - \mathbf{U}_{n-1}^k], \quad (4b)$$

for $n = 1, \dots, N$, where $k = 0, 1, 2, \dots$ is the iteration number. This system contains the unknown solutions \mathbf{u}_n and their partial derivatives, which even if known, would be computationally expensive to calculate.

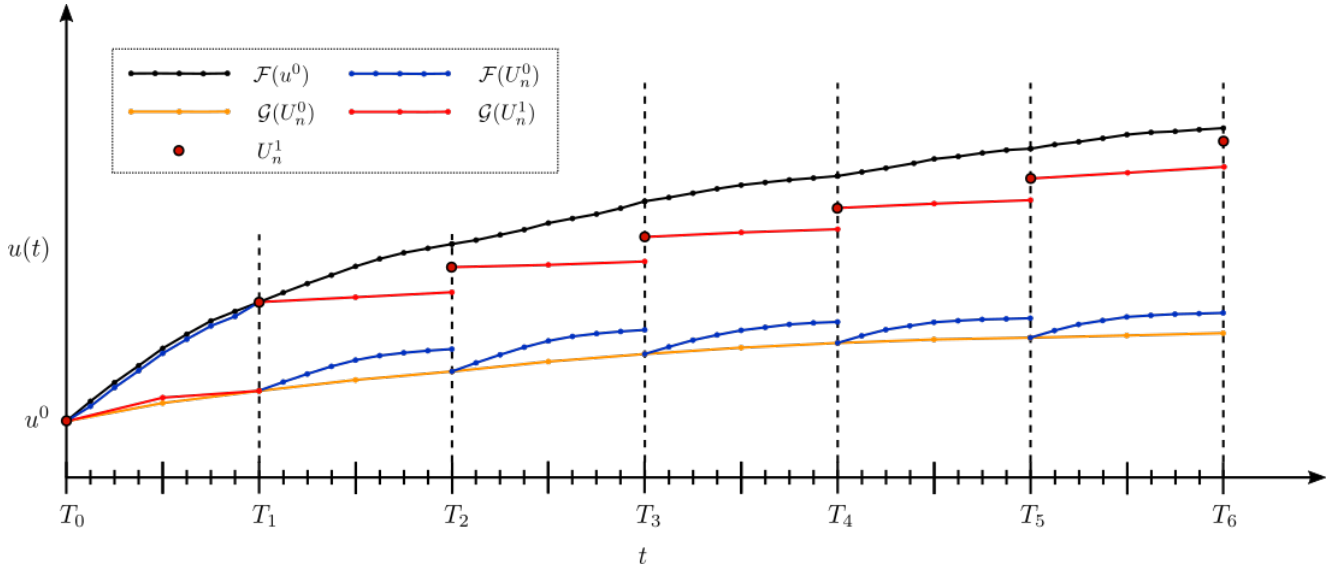


Figure 2: First iteration of the parareal algorithm to numerically evaluate the true solution of a single ODE (black line), either available or obtained via the fine solver. The first runs of \mathcal{G} and \mathcal{F} are given in yellow and blue respectively; and the second run of \mathcal{G} in red. The red dots represent the solution after applying the predictor-corrector (5).

To solve (4) and evaluate \mathbf{u}_n at discrete times, \mathcal{P} utilises two numerical integrators. The first is a numerically fast *coarse integrator* \mathcal{G} that integrates over $[T_n, T_{n+1}]$ using initial values \mathbf{U}_n . The second is a *fine integrator* \mathcal{F} that runs much slower compared to \mathcal{G} but has much greater numerical accuracy, chosen such that it integrates over the same interval $[T_n, T_{n+1}]$ with initial values \mathbf{U}_n . In our implementation, the difference between fast and slow integration is guaranteed by setting the time steps for \mathcal{G} and \mathcal{F} as δT

and δt respectively with $\delta t \ll \delta T$ (recall Figure 1). The key principle is that, if used to integrate (1) over $[T_0, T_N]$ serially, \mathcal{F} would take an infeasible amount of computational time, hence the need to use \mathcal{P} in the first place. Therefore \mathcal{G} is permitted to run serially across multiple sub-intervals rapidly, whereas the slower solver \mathcal{F} is only permitted to run in parallel on sub-intervals. This is a strict requirement for running \mathcal{P} , else numerical speed-up will not be achieved.

Given that (4a) is known *a priori* for all k , Lions et al. [8] approximate the first term in equation (4b) using the fine solver $\mathcal{F}(\mathbf{U}_{n-1}^k)$ and the second term by a coarse finite difference of the derivative using $\mathcal{G}(\mathbf{U}_{n-1}^{k+1}) - \mathcal{G}(\mathbf{U}_{n-1}^k)$. The result is that an initial guess for the initial values \mathbf{U}_n^0 (found using \mathcal{G}) is improved at successive parareal iterations k using the predictor-corrector update rule

$$\mathbf{U}_n^{k+1} = \mathcal{F}(\mathbf{U}_{n-1}^k) + \mathcal{G}(\mathbf{U}_{n-1}^{k+1}) - \mathcal{G}(\mathbf{U}_{n-1}^k) \quad \text{for } n = 1, \dots, N. \quad (5)$$

Pseudocode for an implementation of \mathcal{P} is given in Algorithm 1 alongside a graphical description of the first iteration in Figure 2. During the ‘zeroth’ iteration, \mathcal{G} is applied to \mathbf{u}^0 , generating initial values $\hat{\mathbf{U}}_n^0 \forall n \in \{1, \dots, N\}$ sequentially (lines 1-6). Immediately following, \mathcal{F} is run in parallel from these initial values to generate a more accurate set of fine solution states $\hat{\mathbf{U}}_n^0$ (lines 8-11). Next, \mathcal{G} is run in the first time sub-interval, from the known initial value, to ‘predict’ the solution $\hat{\mathbf{U}}_1^1$ at T_1 . It is subsequently ‘corrected’ using rule (5), and the predictor-corrector solution \mathbf{U}_1^1 is found at T_1 . This prediction and correction process (lines 12-16) repeats sequentially in each sub-interval until \mathbf{U}_n^1 is found $\forall n \in \{1, \dots, N\}$. After checking if the stopping criteria has been met (lines 17-21), the algorithm either starts the next iteration or stops.

2.1 Stopping criteria and other properties

The algorithm is said to have converged up to time T_I if

$$\|\mathbf{U}_n^k - \mathbf{U}_n^{k-1}\|_\infty < \varepsilon \quad \forall n \leq I, \quad (6)$$

for some small fixed tolerance ε [21, 17]. Note that $\|\cdot\|_\infty$ denotes the usual infinity norm. Once $I = N$, we say \mathcal{P} has taken $k_d = k$ iterations to converge, yielding a solution with numerical accuracy of the order of the \mathcal{F} solver. Alternative stopping criteria such as comparing the results of the coarse and fine solvers at successive iterations can be used. In its original formulation, \mathcal{P} iteratively improves the solution across *all* time steps, regardless of whether they have converged or not, up until convergence has been met for all T_n . The modified formulation presented here however only iterates on the solutions for the unconverged sub-intervals [23, 17]. This has no effect on the convergence rate k_d and becomes especially important once we introduce the stochastic modifications in section 3.

It should be clear that *at least* one sub-interval will converge during each iteration k , as \mathcal{F} will be run directly from a converged initial value. For example, during the first iteration, \mathcal{F} is run directly from the initial values at T_0 and hence the solution in $[T_0, T_1]$ converges immediately. Therefore it will take at most $k_d = N$ iterations for \mathcal{P} to converge, equivalent to running \mathcal{F} over the N sub-intervals serially (i.e. no parallel speed-up). To achieve significant parallel speed-up, multiple sub-intervals need to converge during an iteration so that convergence occurs in $k_d \ll N$ iterations. Assuming \mathcal{G} takes a negligible amount of time to run compared to the parallel components (along with any other serial computations), the approximate parallel speed-up achieved by \mathcal{P} is then N/k_d .

One challenge in attempting to minimise k_d , hence the overall runtime of \mathcal{P} , is to identify optimal solvers \mathcal{F} and \mathcal{G} for implementation. Whereas \mathcal{F} is assumed to be accurate and computationally expensive to run, \mathcal{G} must be chosen such that it runs significantly faster (usually orders of magnitude) than \mathcal{F}

Algorithm 1 Parareal (\mathcal{P})

```

1: Set counters  $k = I = 0$  and define  $\mathbf{U}_n^k$ ,  $\hat{\mathbf{U}}_n^k$  and  $\tilde{\mathbf{U}}_n^k$  as the predictor-corrector, coarse, and fine solutions
   at the  $n^{th}$  time step and  $k^{th}$  iteration respectively (note that  $\mathbf{U}_0^k = \hat{\mathbf{U}}_0^k = \tilde{\mathbf{U}}_0^k = \mathbf{u}^0 \forall k$ ).
2: // Calculate initial values at the start of each sub-interval  $T_n$  by running  $\mathcal{G}$  serially on processor  $P_1$ .
3: for  $n = 1$  to  $N$  do
4:    $\hat{\mathbf{U}}_n^0 = \mathcal{G}(\hat{\mathbf{U}}_{n-1}^0)$ 
5:    $\mathbf{U}_n^0 = \hat{\mathbf{U}}_n^0$ 
6: end for
7: for  $k = 1$  to  $N$  do
8:   // Propagate the predictor-corrector solutions (from iteration  $k - 1$ ) on each sub-interval by running
    $\mathcal{F}$  in parallel on processors  $P_{I+1}, \dots, P_N$ .
9:   for  $n = I + 1$  to  $N$  do
10:     $\tilde{\mathbf{U}}_n^{k-1} = \mathcal{F}(\mathbf{U}_{n-1}^{k-1})$ 
11:   end for
12:   // Propagate the predictor-corrector solution (at iteration  $k$ ) with  $\mathcal{G}$  on any available processor.
   Then correct this value using coarse and fine solutions obtained during iteration  $k - 1$  (this step
   cannot be carried out in parallel).
13:   for  $n = I + 1$  to  $N$  do
14:     $\hat{\mathbf{U}}_n^k = \mathcal{G}(\mathbf{U}_{n-1}^k)$ 
15:     $\mathbf{U}_n^k = \tilde{\mathbf{U}}_n^{k-1} + \hat{\mathbf{U}}_n^k - \hat{\mathbf{U}}_n^{k-1}$ 
16:   end for
17:   // Check whether the stopping criterion is met, saving all solutions up to time step  $T_I$  before the
   next iteration. If tolerance is met for all time steps, the algorithm stops.
18:    $I = \max_{n \in \{I+1, \dots, N\}} \|\mathbf{U}_i^k - \mathbf{U}_i^{k-1}\|_\infty < \varepsilon \forall i < n$ 
19:   if  $I == N$  then
20:     return  $k, \mathbf{U}^k$ 
21:   end if
22: end for

```

to minimise the runtime of the sequential parts of the algorithm, whilst being sufficiently numerically accurate to converge in as few iterations as possible. Potential choices for the coarse solver include integrators with reduced physics or coarser spatial resolutions (when solving PDEs), or using the same integrator as \mathcal{F} with much coarser time steps. There is currently no rigorous method for choosing the two solvers. However, they should be chosen such that the ratio between the time taken to run the \mathcal{F} solver over $[T_n, T_{n+1}]$ and the time taken to run the \mathcal{G} solver over the same interval is large.

In this paper, we fix both \mathcal{F} and \mathcal{G} as explicit¹ fourth-order Runge-Kutta methods (henceforth RK4) for ease of implementation, and to allow us to directly compare and contrast performances in [section 4](#). More detailed analysis on the mathematical conditions required for \mathcal{P} to converge, i.e. for the numerical solution \mathbf{U}_n to approach the true solution \mathbf{u} , can be found in [\[25, 20, 8, 22\]](#).

3 A stochastic parareal algorithm

In this section we introduce the stochastic parareal algorithm, an extension of parareal that incorporates randomness and utilises its well-studied deterministic convergence properties to locate a solution in $k_s \leq k_d$ iterations. A summary of additional notation required to describe the algorithm, henceforth referred to as \mathcal{P}_s , is provided in [Table 1](#).

The idea behind \mathcal{P}_s is to sample M vectors of initial values $\alpha_{n,1}^k, \dots, \alpha_{n,M}^k$, at each unconverged sub-interval T_n , in the neighbourhood of the current predictor-corrector solution \mathbf{U}_n^k from a given probability distribution, and propagate them all in parallel using \mathcal{F} . Given a sufficient number of samples is taken, and the distribution has broad enough support, one will be closer (in the Euclidean sense) to the true root that equation (5) is converging toward. Among them, we select an optimal $\hat{\alpha}_n^k$ by identifying which samples generate the most continuous trajectory, at the fine resolution, in phase space across $[T_0, T_N]$. Therefore, at each iteration, we stochastically “jump” toward more accurate initial values that are then fed into the predictor-corrector (5). For increasing values of M , the convergence rate k_s will decrease, satisfying $k_s \leq k_d$ with some probability, as shown in [section 4](#).

3.1 The algorithm

Suppose again we aim to solve system (1), adopting the same conditions, properties, and notation as discussed in [section 2](#). \mathcal{P}_s follows the first iteration ($k = 1$) of \mathcal{P} identically - see line 1 of [Algorithm 2](#). This is because information about initial values at the different temporal resolutions (i.e. results from \mathcal{F} and \mathcal{G}) are required to construct the appropriate probability distributions for sampling. Following the convergence check, we assume (for the purposes of explaining the stochastic iterations) that only the first sub-interval $[T_0, T_1]$ converged during $k = 1$, leaving $N - 1$ unconverged sub-intervals. At this point we know the most up-to-date predictor-corrector solutions $\mathbf{U}_n^1 \forall n \in \{1, \dots, N\}$ and the stochastic iterations can begin (henceforth $k = 2$).

At any unconverged T_n ($n > 1$), we sample M vectors of initial values, denoted $\alpha_{n,m}^{k-1}$ for $m = 1, \dots, M$. The first is fixed as the predictor-corrector value \mathbf{U}_n^{k-1} , to ensure that $\mathcal{P}_s = \mathcal{P}$ when $M = 1$. The other $M - 1$ initial values are sampled from a pre-specified d -dimensional probability distribution Φ_n^{k-1} with finite marginal means $\mu_n^{k-1} = (\mu_{n_1}^{k-1}, \dots, \mu_{n_d}^{k-1})^T$, standard deviations $\sigma_n^{k-1} = (\sigma_{n_1}^{k-1}, \dots, \sigma_{n_d}^{k-1})^T$, and correlation structure given by the matrix \mathbf{R}_n^{k-1} . These quantities depend upon the information available at iteration

¹Use of an implicit solver would provide greater numerical stability at extra computational cost. For simplicity and speed we use explicit solvers with sufficiently small time steps to ensure numerical stability when solving the stiff ODE systems in [section 4](#).

Table 1: Additional notation used to describe the stochastic parareal algorithm.

Notation	Description
n	Index of the time sub-interval T_n , $n = 0, \dots, N$.
k	Iteration number of \mathcal{P} and \mathcal{P}_s , $k = 1, \dots, N$.
k_s	Total iterations taken for stochastic parareal to stop and return a solution, $k_s \in \{1, \dots, N\}$.
M	Number of random samples taken at each T_n .
Φ_n^{k-1}	The d -dimensional probability distribution used to sample initial values at time T_n and iteration k .
$\alpha_{n,m}^{k-1}$	The m^{th} d -dimensional sample from distribution Φ_n^{k-1} at time T_n and iteration k , $m = 1, \dots, M$.
$\hat{\alpha}_n^{k-1}$	The selected d -dimensional sample from $\alpha_{n,1}^{k-1}, \dots, \alpha_{n,M}^{k-1}$ at time T_n and iteration k .
μ_n^{k-1}	The d -dimensional vector of marginal means at time T_n and iteration k .
σ_n^{k-1}	The d -dimensional vector of marginal standard deviations at time T_n and iteration k .
$\rho_{n,i,j}^{k-1}$	Pairwise correlations coefficients between i^{th} and j^{th} components of the M fine resolution propagated samples at time T_n and iteration k .
\mathbf{R}_n^{k-1}	The symmetric positive semi-definite $d \times d$ correlation matrix with elements $\rho_{n,i,j}^{k-1}$ at time T_n and iteration k .
\mathbb{I}	The $d \times d$ identity matrix.
Σ_n^{k-1}	The symmetric positive semi-definite $d \times d$ covariance matrix at time T_n and iteration k .

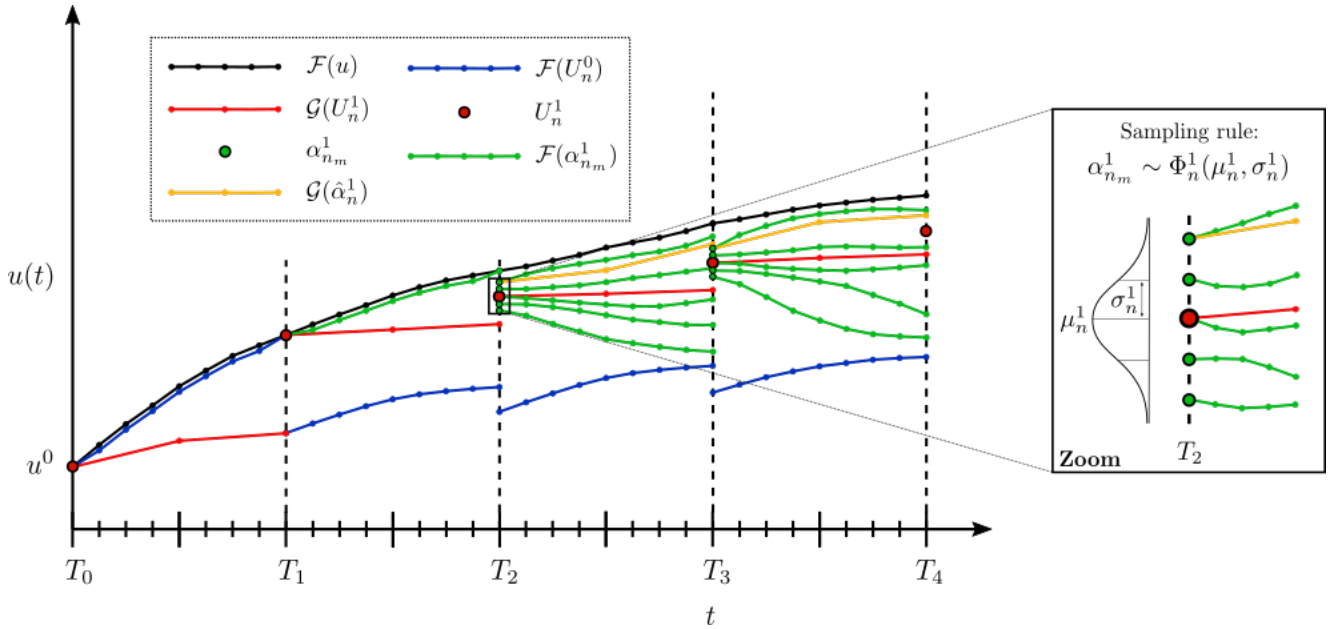


Figure 3: A depiction of the sampling and propagation process within \mathcal{P}_s following iteration $k = 1$. The fine solution is given in black, the $k = 0$ fine solutions in blue, the $k = 1$ coarse solutions in red, and the $k = 1$ predictor-corrector solutions as red dots. With $M = 5$, four samples $\alpha_{n,m}^1$ (green dots) are taken at T_2 and T_3 from distributions with means U_2^1 and U_3^1 , and some finite standard deviations respectively. These values, along with U_2^1 and U_3^1 themselves, are propagated in parallel forward in time using \mathcal{F} (green lines). The optimally chosen samples $\hat{\alpha}_n^1$ (refer to text for how these are chosen) are then propagated forward in time using \mathcal{G} (yellow lines).

$k-1$, i.e. a combination of \mathbf{U}_n^{k-1} , $\mathcal{F}(\mathbf{U}_n^{k-1})$, $\mathcal{G}(\mathbf{U}_n^{k-1})$ and $\mathcal{G}(\mathbf{U}_n^{k-2})$, see [section 3.3](#). The correlation matrix is introduced for taking into account the dependence between the components of the system of ODEs. The elements

$$(\mathbf{R}_n^{k-1})_{i,j} = \begin{cases} 1 & \text{if } i = j \\ \rho_{n,i,j}^{k-1} & \text{if } i \neq j \end{cases}, \text{ for } k \geq 3 \quad (7)$$

are the estimated pairwise correlation coefficients of the M d -dimensional fine resolution propagations of the sampled initial values $\mathcal{F}(\alpha_{n-1,1}^{k-2}), \dots, \mathcal{F}(\alpha_{n-1,M}^{k-2})$ at T_n from the previous iteration (lines 3-9). Since $\mathcal{F}(\alpha_{n-1,i}^{k-2})$, $i = 1, \dots, M$, are not available at iteration $k = 2$, we set $\mathbf{R}_n^{k-1} = \mathbb{I}$ for each n , i.e. we sample from a multivariate distribution with uncorrelated components.

Following this, the sampling and subsequent propagation using \mathcal{F} can begin in parallel (lines 10-22). Given the solution between $[T_0, T_1]$ has converged, \mathcal{F} will run from the converged initial value at T_1 , with sampling starting from T_2 onward (see [Figure 3](#)). All sampled initial values are then propagated forward in parallel using \mathcal{F} , requiring at least $M(N-2) + 1$ processors (M samples times $N-2$ unconverged sub-intervals plus running \mathcal{F} once in $[T_1, T_2]$).

Of the M sampled initial values at each T_n ($n > 1$), only one is retained, denoted by $\hat{\alpha}_n^{k-1}$, chosen such that it minimises the Euclidean distance between the fine solution and the sampled values (lines 23-28). To do this, start from the converged initial values at T_2 given by the fine solver: $\mathcal{F}(\mathbf{U}_1^{k-1})$. Calculate the Euclidean distance between $\mathcal{F}(\mathbf{U}_1^{k-1})$ and each of the M samples $\alpha_{2,1}^{k-1}, \dots, \alpha_{2,M}^{k-1}$. The sample minimising this distance is chosen as $\hat{\alpha}_2^{k-1}$. Repeat for later T_n , minimising the distance between $\mathcal{F}(\hat{\alpha}_{n-1}^{k-1})$ and one of the samples $\alpha_{n,1}^{k-1}, \dots, \alpha_{n,M}^{k-1}$. This process must be run sequentially and relies on the modification to \mathcal{P} made in [section 2](#) - that solutions are not altered once converged. Referring again to [Figure 3](#), the corresponding coarse trajectories of these optimally chosen samples $\hat{\alpha}_n^{k-1}$ must also be calculated to carry out the predictor-corrector step (lines 29-32).

At this point, the set of initial values $\{\hat{\alpha}_2^{k-1}, \dots, \hat{\alpha}_{N-1}^{k-1}\}$ has been selected from the ensemble of random samples, effectively replacing the previously found \mathbf{U}_n^{k-1} . The coarse and fine propagations of these values are now used in the predictor-corrector (lines 33-37) such that

$$\mathbf{U}_n^k = \begin{cases} \mathcal{F}(\mathbf{U}_{n-1}^{k-1}) + \mathcal{G}(\mathbf{U}_{n-1}^k) - \mathcal{G}(\mathbf{U}_{n-1}^{k-1}) & \text{for } n = 2, \\ \mathcal{F}(\hat{\alpha}_{n-1}^{k-1}) + \mathcal{G}(\mathbf{U}_{n-1}^k) - \mathcal{G}(\hat{\alpha}_{n-1}^{k-1}) & \text{for } n = 3, \dots, N. \end{cases} \quad (8)$$

Using the same stopping criteria (6) from \mathcal{P} (lines 38-42), the algorithm either stops or runs another stochastic parareal iteration.

3.2 Features and properties

Before detailing the sampling distributions deployed within \mathcal{P}_s , we present a few key features and properties of the algorithm:

- Upon independent repeated simulations, \mathcal{P}_s will yield a numerical solution to system (1) which, along with k_s , will vary stochastically. Since chosen trajectories vary depending on which optimal initial values are determined during a particular simulation. The median solution (calculated upon multiple realisations) does however retain numerical accuracy when compared to the solution from \mathcal{P} , and hence the fine solver. To measure the performance in terms of the convergence rate, we estimate the discrete distributions of k_s by running \mathcal{P}_s at least 10^3 times for different M .

- \mathcal{P}_s runs \mathcal{F} more frequently than \mathcal{P} and hence requires more processors. The first iteration of \mathcal{P}_s requires N processors, however once sampling begins in $k = 2$, it requires at most $M(N - I - 1) + 1$ processors - assuming I sub-intervals converge during $k = 1$. Whilst we assume processors are in abundance, this number scales directly with M and hence it is important to keep M to a minimum.
- The runtime of an iteration in \mathcal{P}_s is comparable to one in \mathcal{P} , given that the calculation of correlations, selecting the optimal samples, and the extra \mathcal{G} runs, have negligible serial runtimes.

3.3 Sampling rules

The chosen sampling distributions Φ_n^{k-1} incorporate different combinations of available information about the initial values at different temporal resolutions, i.e. the coarse, fine, and predictor-corrector initial values $\mathcal{G}(\mathbf{U}_{n-1}^{k-1})$, $\mathcal{G}(\mathbf{U}_{n-1}^{k-2})$, $\mathcal{F}(\mathbf{U}_{n-1}^{k-2})$, and \mathbf{U}_n^{k-1} respectively, $\forall n \in \{1, \dots, N\}$. This information is used to define the marginal means and standard deviations in the ‘sampling rules’ outlined in the following subsections. Note how the distributions vary with time T_n and k , so that the accuracy of the distributions increase as the initial values in \mathcal{P}_s are iteratively improved. Using Gaussian and copula distributions, we analyse the performance of multiple ‘sampling rules’ within \mathcal{P}_s in [section 4](#). This will give us a more comprehensive understanding on whether the choice of distribution family Φ_n^{k-1} or its parameters μ_n^{k-1} , σ_n^{k-1} , and \mathbf{R}_n^{k-1} has the greatest impact on the convergence rate k_s . In all tested cases, we show how the inclusion of correlations between components, estimated using Pearson correlation coefficients, significantly improves the performance of \mathcal{P}_s with respect to the independent setting.

3.3.1 Multivariate Gaussian

First, we consider perturbing the initial values using stochastic “noise”, i.e. considering errors compared to the true initial values to be normally distributed, a standard method for modelling uncertainty. Therefore, the initial values $\alpha_{n,m}^{k-1}$ are sampled from a multivariate Gaussian distribution $\mathcal{N}(\mu_n^{k-1}, \Sigma_n^{k-1})$, where Σ_n^{k-1} is the $d \times d$ positive semi-definite covariance matrix with elements $\rho_{n,i,j}^{k-1} \sigma_{n_i}^{k-1} \sigma_{n_j}^{k-1}$ for $i, j = 1, \dots, d$. As marginal means μ_n^{k-1} we choose either the fine resolution values $\mathcal{F}(\mathbf{U}_{n-1}^{k-2})$ (prior to correction) or the predictor-corrector values \mathbf{U}_n^{k-1} . For the standard deviations, we choose $\sigma_n^{k-1} = |\mathcal{G}(\mathbf{U}_{n-1}^{k-1}) - \mathcal{G}(\mathbf{U}_{n-1}^{k-2})|$ because they are of the order of the corrections made by the predictor-corrector at each T_n . Note that $|\cdot|$ denotes the component-wise absolute value. Testing revealed that alternative standard deviations $|\mathbf{U}_n^{k-1} - \mathbf{U}_n^{k-2}|$ and $|\mathcal{F}(\mathbf{U}_{n-1}^{k-2}) - \mathcal{G}(\mathbf{U}_{n-1}^{k-2})|$ did not span sufficiently large distances around μ_n^{k-1} in order for sampling to be efficient, i.e they required much higher sampling to perform as well as $\sigma_n^{k-1} = |\mathcal{G}(\mathbf{U}_{n-1}^{k-1}) - \mathcal{G}(\mathbf{U}_{n-1}^{k-2})|$ (results not shown). The Gaussian sampling rules are therefore defined as $\alpha_{n,m}^{k-1} \sim \mathcal{N}(\mu_n^{k-1}, \Sigma_n^{k-1})$ using the following parameters:

Rule 1: $\mu_n^{k-1} = \mathcal{F}(\mathbf{U}_{n-1}^{k-2})$ and $\sigma_n^{k-1} = |\mathcal{G}(\mathbf{U}_{n-1}^{k-1}) - \mathcal{G}(\mathbf{U}_{n-1}^{k-2})|$.

Rule 2: $\mu_n^{k-1} = \mathbf{U}_n^{k-1}$ and $\sigma_n^{k-1} = |\mathcal{G}(\mathbf{U}_{n-1}^{k-1}) - \mathcal{G}(\mathbf{U}_{n-1}^{k-2})|$.

Linearly combining the means from both rules or taking half the samples from each appears to work well, with performance similar to the individual rules themselves (results not shown).

3.3.2 Multivariate copula

Alternatively, we consider modelling errors that may have a different (non-Gaussian) dependency structure. We therefore consider another multivariate distribution, with uniform marginals scaled such that

they have the same marginal means and standard deviations as the Gaussian. Such distributions are known as copulas.

A copula $\mathcal{C} : [0, 1]^d \rightarrow [0, 1]$ is a joint cumulative distribution function (CDF), of a d -dimensional random vector, with uniform marginal distributions [26]. Sklar's theorem [27] states that any multivariate CDF can be written in terms of d uniform marginal distributions and a copula that describes the correlation structure between them. Whilst there are numerous families of copulas, we consider the symmetric t -copula, \mathcal{C}^t , the copula underlying the multivariate t -distribution, which depends on the degrees of freedom parameter ν and the correlation matrix \mathbf{R}_n^{k-1} . We fix $\nu = 1$ so that samples have a higher probability of being drawn toward the edges of the $[0, 1]^d$ hypercube, see [26]. Note that $\nu \rightarrow \infty$ can be thought of as sampling from the Gaussian copula.

Correlated samples $\chi = (\chi_1, \dots, \chi_d)^T \sim \mathcal{C}^t$ that are generated in $[0, 1]^d$ then need to be re-scaled such that each marginal is uniformly distributed in an interval $[x_i, y_i] \subset \mathbb{R}$, with mean μ_i and standard deviation σ_i for $i \in \{1, \dots, d\}$. By definition, a marginal uniform distribution on $[x_i, y_i]$ has mean $(x_i + y_i)/2$ and variance $(y_i - x_i)^2/12$ which we set to μ_i and σ_i^2 respectively. Solving these equations, we find that the desired marginals are uniform distributions in $[\mu_i - \sqrt{3}\sigma_i, \mu_i + \sqrt{3}\sigma_i]$ for $i \in \{1, \dots, d\}$. Thus, scaling by $2\sqrt{3}\sigma_i\chi_i + \mu_i - \sqrt{3}\sigma_i$ guarantees that the generated samples $\chi \sim \mathcal{C}^t$ have the same marginal means μ_i and standard deviations σ_i as the Gaussian distributions. This allows us to compare performance results in section 4. The t -copula sampling rules (**Rule 3** and **Rule 4**) are thus defined component-wise as $(\alpha_{n,m}^{k-1})_i = 2\sqrt{3}\sigma_i\chi_i + \mu_i - \sqrt{3}\sigma_i$, for $i \in \{1, \dots, d\}$, with $\chi \sim \mathcal{C}^t$ and parameters identical to Rule 1 and Rule 2 respectively.

Algorithm 2 Stochastic parareal (\mathcal{P}_s)

```

1: Run  $\mathcal{P}$  until the end of iteration  $k = 1$ .
2: for  $k = 2$  to  $N$  do
3:   // Calculate correlation matrices (only if  $d > 1$ ).
4:    $\mathbf{R}_n^{k-1} = \mathbb{I} \forall n$ 
5:   if  $k \geq 3$  then
6:     for  $n = I + 1$  to  $N - 1$  do
7:       Calculate  $\mathbf{R}_n^{k-1}$  using  $\mathcal{F}(\alpha_{n-1,1}^{k-2}), \dots, \mathcal{F}(\alpha_{n-1,M}^{k-2})$ .
8:     end for
9:   end if
10:  // Initial value sampling and propagation on processors  $P_1, \dots, P_{M(N-I-1)+1}$  (note both for loops
    should be run in parallel).
11:  for  $n = I$  to  $N - 1$  do
12:    if  $n == I$  then
13:       $\tilde{\mathbf{U}}_{n+1}^{k-1} = \mathcal{F}(\mathbf{U}_n^{k-1})$  // propagation from the converged initial value at  $T_I$ 
14:    else
15:       $\alpha_{n,1}^{k-1} = \mathbf{U}_n^{k-1}$  // first sample is set as the predictor-corrector value
16:       $\tilde{\mathbf{U}}_{n+1,1} = \mathcal{F}(\alpha_{n,1}^{k-1})$  // propagated values stored in temporary variable
17:      for  $m = 2$  to  $M$  do
18:         $\alpha_{n,m}^{k-1} \sim \Phi_n^{k-1}$  //  $M - 1$  samples randomly selected
19:         $\tilde{\mathbf{U}}_{n+1,m} = \mathcal{F}(\alpha_{n,m}^{k-1})$ 
20:      end for
21:    end if
22:  end for
23:  // Select the most continuous fine trajectory from the ensemble sequentially.
24:  for  $n = I + 1$  to  $N - 1$  do
25:     $J = \operatorname{argmin}_{j \in \{1, \dots, M\}} \|\alpha_{n,j}^{k-1} - \tilde{\mathbf{U}}_n^{k-1}\|_2$ 
26:     $\hat{\alpha}_n^{k-1} = \alpha_{n,J}^{k-1}$  // store optimal initial value
27:     $\tilde{\mathbf{U}}_{n+1}^{k-1} = \tilde{\mathbf{U}}_{n+1,J}$  // store most optimal fine trajectories
28:  end for
29:  // Run  $\mathcal{G}$  from the optimal samples (can run in parallel).
30:  for  $n = I + 1$  to  $N - 1$  do
31:     $\hat{\mathbf{U}}_{n+1}^{k-1} = \mathcal{G}(\hat{\alpha}_n^{k-1})$ 
32:  end for
33:  // Predict and correct the initial values using (5).
34:  for  $n = I + 1$  to  $N$  do
35:     $\hat{\mathbf{U}}_n^k = \mathcal{G}(\mathbf{U}_{n-1}^k)$ 
36:     $\mathbf{U}_n^k = \tilde{\mathbf{U}}_n^{k-1} + \hat{\mathbf{U}}_n^k - \hat{\mathbf{U}}_n^{k-1}$ 
37:  end for
38:  // Check whether the stopping criterion is met.
39:   $I = \max_{n \in \{I+1, \dots, N\}} \|\mathbf{U}_i^k - \mathbf{U}_i^{k-1}\|_\infty < \varepsilon \forall i < n$ 
40:  if  $I == N$  then
41:    return  $k, \mathbf{U}^k$ 
42:  end if
43: end for

```

4 Numerical results

In the following section we compare the numerical performance of \mathcal{P} and \mathcal{P}_s on systems of one, two, and three ODEs with varying complexity and dynamical properties. Both algorithms will use RK4 methods to carry out integration, with \mathcal{G} using time step δT and \mathcal{F} using time step δt , the latter at least 75 times smaller than the former. We quantify the performance of \mathcal{P}_s by estimating the distributions of k_s for the different sampling rules, and measuring the accuracy of the stochastic solutions against those given serially by \mathcal{F} . All algorithms were coded in MATLAB and simulations were run using HPC facilities at the University of Warwick. Samples code for both algorithms can be found in a public repository². Since a limited number of processors were available for these experiments, the results are based not on calculating wallclock runtimes but on comparing the convergence rates k_d and k_s - which are independent of the number of processors used. Additional results for the problems here, as well as two further test problems, are given in the Appendix.

4.1 One-dimensional nonlinear equation

First, we consider the nonlinear ODE

$$\frac{du_1}{dt} = \sin(u_1)\cos(u_1) - 2u_1 + e^{-t/100}\sin(5t) + \ln(1+t)\cos(t), \quad (9)$$

with initial value $u_1(0) = 1$ [7]. Discretise the time interval $t \in [0, 100]$ using $N = 40$ sub-intervals, coarse time steps $\delta T = 100/80$, and fine time steps $\delta t = 100/8000$. Numerical solutions to (9) are shown on the interval $[0, 18]$ in Figure 4a. Deterministically, \mathcal{P} locates a solution in $k_d = 25$ iterations using error tolerance $\varepsilon = 10^{-10}$. \mathcal{P}_s converges in a varying number of iterations $k_s < k_d$ - see Figure 4b for the convergence of ten independent simulations using just $M = 2$. From this plot, with just two samples, \mathcal{P}_s already betters k_d by up to ten iterations.

When M is increased above one, \mathcal{P}_s begins generating stochastic solutions that converge in a varying number of iterations k_s . In order to accurately compare k_d with the discrete random variable k_s , we run 2000 independent simulations of \mathcal{P}_s to estimate the distribution of k_s for a given M . Upon estimating these distributions, it was found that $\mathbb{P}(k_s < 25) = 1$ for each of the four sampling rules (for all $M > 1$). The distributions estimated, using sampling rule 1 (the other rules perform similarly), as a function of M are given in Figure 5a. The stacked bars represent the estimated discrete probability of a simulation converging in a given number of iterations. The results show \mathcal{P}_s converging in just five iterations in the best case - demonstrating \mathcal{P}_s has the potential to yield significant parallel speed-up, given sufficiently many samples are drawn. Figure 5b emphasises the power of the stochastic method, showing that the expected value of k_s , $\mathbb{E}(k_s) = \sum_{k=1}^N k\mathbb{P}(k_s = k)$, decreases as M increases. Sampling rule 1 yields the lowest expected values of k_s for small values of M with all sampling rules performing similarly for large M .

To verify the accuracy of the stochastic solutions, absolute differences between 250 independent realisations of \mathcal{P}_s and the serially calculated \mathcal{F} solution were determined - see Figure 6. The standard deviation between all 250 solutions is $\mathcal{O}(10^{-11})$ and the error generated by the median \mathcal{P}_s solution is smaller than that given by \mathcal{P} . See Appendix A for additional numerical results of \mathcal{P}_s applied to a one-dimensional stiff nonlinear ODE problem.

²<https://github.com/kpentland/StochasticParareal>

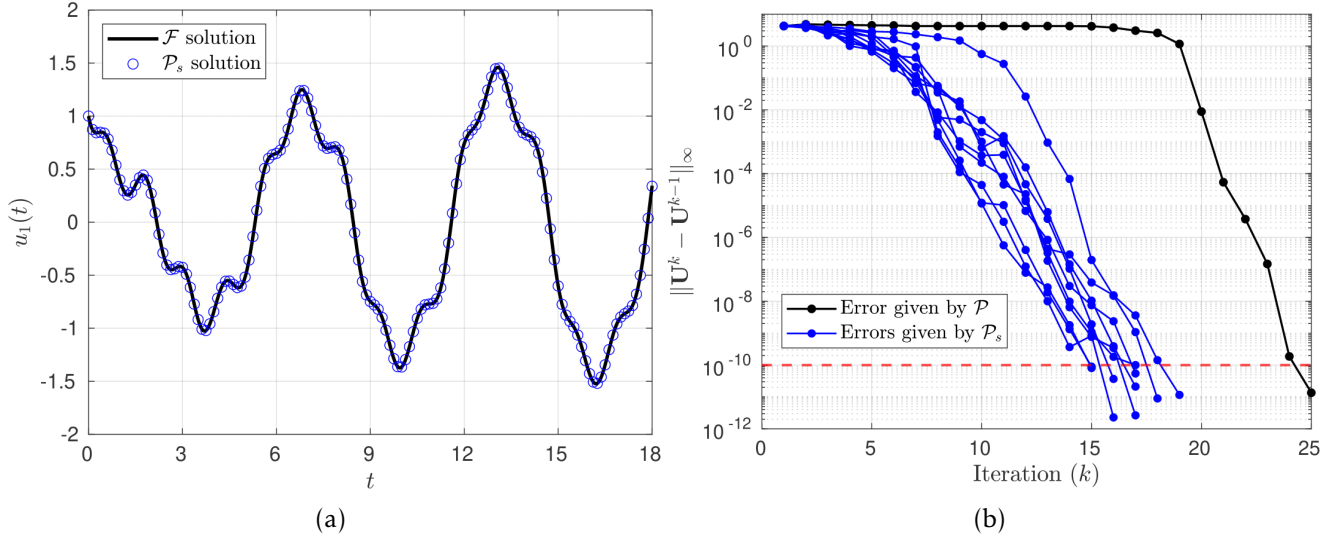


Figure 4: (a) Numerical solution of (9) over $[0,18]$ using \mathcal{F} serially and \mathcal{P}_s . Note that only a subset of the fine times steps of the \mathcal{P}_s solution are shown for clarity. (b) Errors at successive iterations of \mathcal{P} (black line) and ten independent realisations of \mathcal{P}_s (blue lines). Horizontal dashed red line represents the stopping tolerance $\varepsilon = 10^{-10}$. Note that both panels use \mathcal{P}_s with sampling rule 1 and $M = 2$.

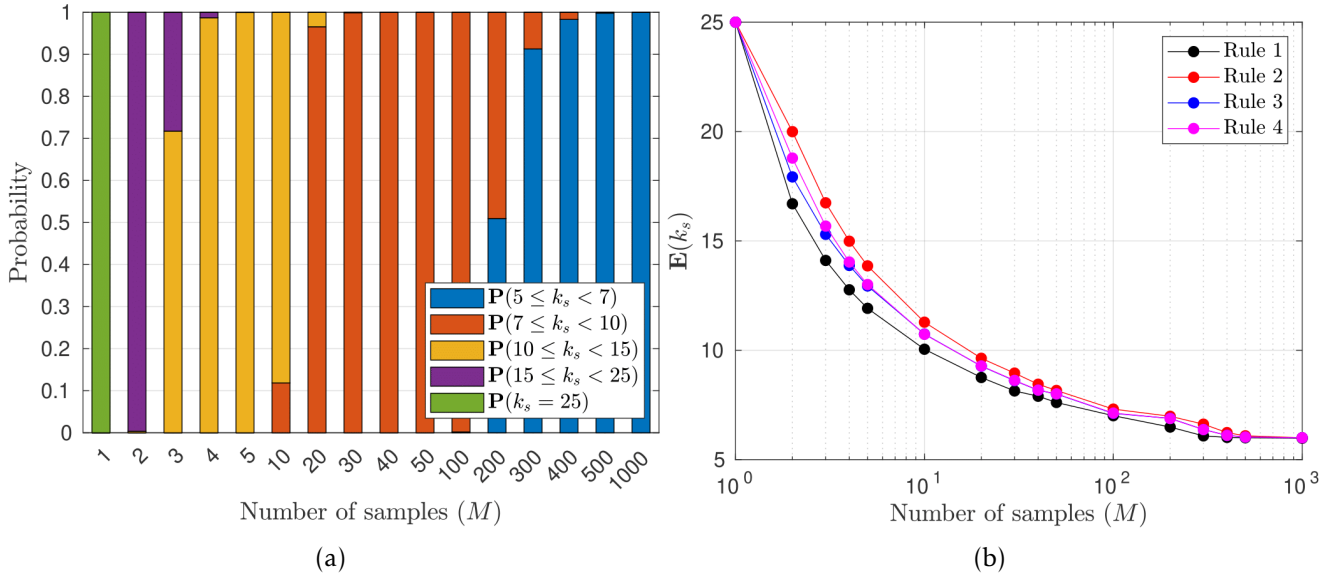


Figure 5: (a) Estimated discrete distributions of k_s as a function of M for sampling rule 1. (b) Estimated expectation of k_s as a function of M , calculated using estimated distributions of k_s for each sampling rule. Distributions in both panels are estimated by simulating 2000 independent realisations of \mathcal{P}_s for each M .

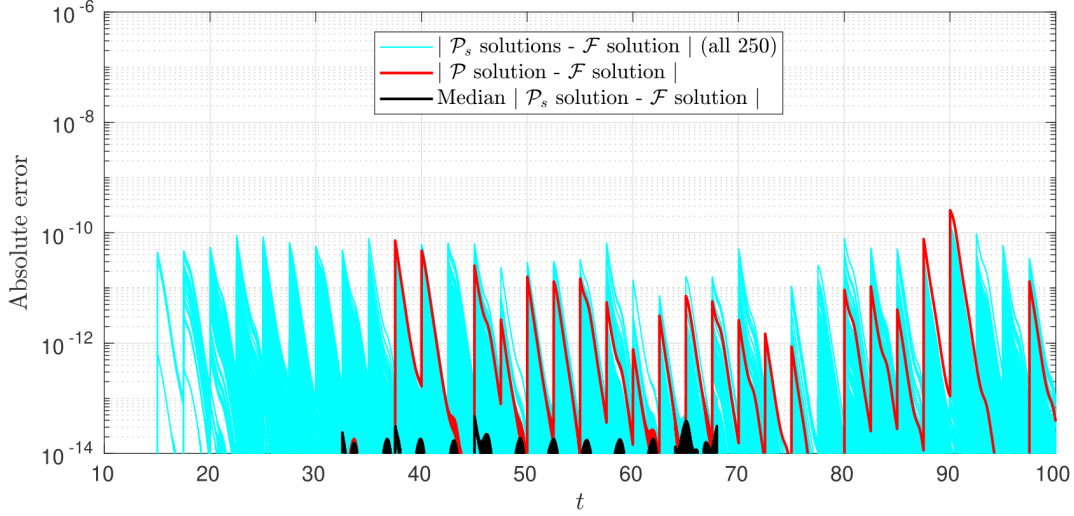


Figure 6: Absolute errors of \mathcal{P} and \mathcal{P}_s against the serial \mathcal{F} solution. Errors obtained from 250 independent realisations of \mathcal{P}_s using sampling rule 2 and $M = 4$ are shown in light blue. The deterministic error generated by \mathcal{P} is shown in red and the median \mathcal{P}_s solution across all 250 simulations in black.

4.2 Two-dimensional Brusselator system

Next, consider the Brusselator system

$$\frac{du_1}{dt} = A + u_1^2 u_2 - (B + 1)u_1, \quad (10a)$$

$$\frac{du_2}{dt} = Bu_1 - u_1^2 u_2, \quad (10b)$$

consisting of a pair of coupled stiff nonlinear ODEs that model an auto-catalytic chemical reaction [28]. Using parameters $A = 1$ and $B = 3$, trajectories of the system exhibit oscillatory behaviour in phase space, approaching a limit cycle (as $t \rightarrow \infty$) that contains the unstable fixed point $(1, 3)^T$. Now that $d > 1$, we use bivariate distributions to sample the initial values - meaning we can compare the effects of including or excluding the correlations between variables. System (10) is solved using initial values $\mathbf{u}(0) = (1, 3.07)^T$ over time interval $t \in [0, 15.3]$ with $N = 25$ sub-intervals and time steps $\delta T = 15.3/25$ and $\delta t = 15.3/2500$ [29]. The numerical solution to (10) in phase space and convergence of the successive errors are reported in Appendix B. With these parameters and a tolerance of $\varepsilon = 10^{-6}$, \mathcal{P} takes $k_d = 7$ iterations to stop and return a numerical solution.

The estimated distributions of k_s for sampling rule 1 are given in Figure 7a. Even though \mathcal{P} takes just $k_d = 7$ iterations to stop, we observe that \mathcal{P}_s can still reach the desired tolerance in 5 or 6 iterations - albeit requiring a large value of M . We suspect this is due to the stiffness of the system and poor accuracy of the explicit \mathcal{G} solver - results presented for stiff systems in Appendix A and Appendix C appear to confirm this. Using adaptive time-stepping methods could be a way to reduce the value of M needed to converge in fewer k_s [24]. The solid lines in Figure 7b show that regardless of which sampling rule is chosen, \mathcal{P}_s only requires $M \approx 10$ to converge in less than seven iterations with probability one. Sampling rules 1 and 3 outperform 2 and 4 in this particular system. Note, however, the stark decrease in performance if instead uncorrelated samples are generated within \mathcal{P}_s (dashed lines). This demonstrates the importance of accounting for the dependence between variables in highly nonlinear systems such as (10). Further

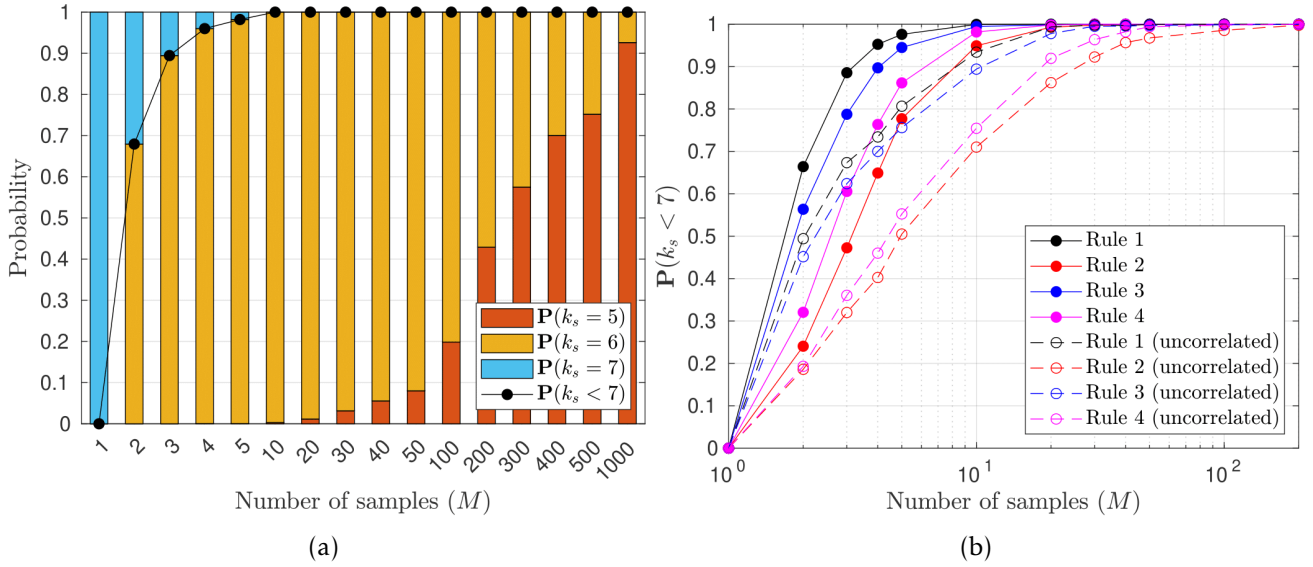


Figure 7: (a) Estimated discrete probabilities of k_s as a function of M for sampling rule 1. (b) Estimated probability that the convergence rate k_s is smaller than $k_d = 7$ as a function of M for the sampling rules with (solid lines) and without (dashed lines) correlations. Distributions were estimated by simulating 2000 independent realisations of \mathcal{P}_s for each M .

results of \mathcal{P}_s applied to (10) and an additional two-dimensional stiff nonlinear system are presented in [Appendix B](#) and [Appendix C](#) respectively.

4.3 Three-dimensional Lorenz system

Finally we consider the Lorenz system

$$\frac{du_1}{dt} = 10(u_2 - u_1), \quad (11a)$$

$$\frac{du_2}{dt} = 28u_1 - u_1u_3 - u_2, \quad (11b)$$

$$\frac{du_3}{dt} = u_1u_2 - \frac{8}{3}u_3, \quad (11c)$$

a simplified model for weather prediction [30]. Trajectories with initial values close to one another diverge exponentially in this regime, giving rise to the notion of a chaotic system. This will test the robustness of \mathcal{P}_s , as small numerical differences between initial values at each sub-interval will result in very different final states, meaning errors can grow rapidly as time progresses. We solve (11) using initial values $\mathbf{u}(0) = (-15, -15, 20)^T$ over the interval $[0, 18]$ which is discretised using $N = 50$ sub-intervals and time steps $\delta T = 18/250$ and $\delta t = 18/18750$. With a tolerance of $\varepsilon = 10^{-8}$, \mathcal{P} takes $k_d = 20$ iterations to converge.

Running \mathcal{P}_s to compare the performance of the sampling rules, we see again in [Figure 8a](#) that taking correlated samples is much more efficient than not. For the chaotic trajectories generated by (11), sampling close to the predictor-corrector, rules 2 and 4, yields superior performance compared to rules 1 and 3 for small values of M . [Figure 8b](#) displays estimated distributions for varying M using sampling rule 2

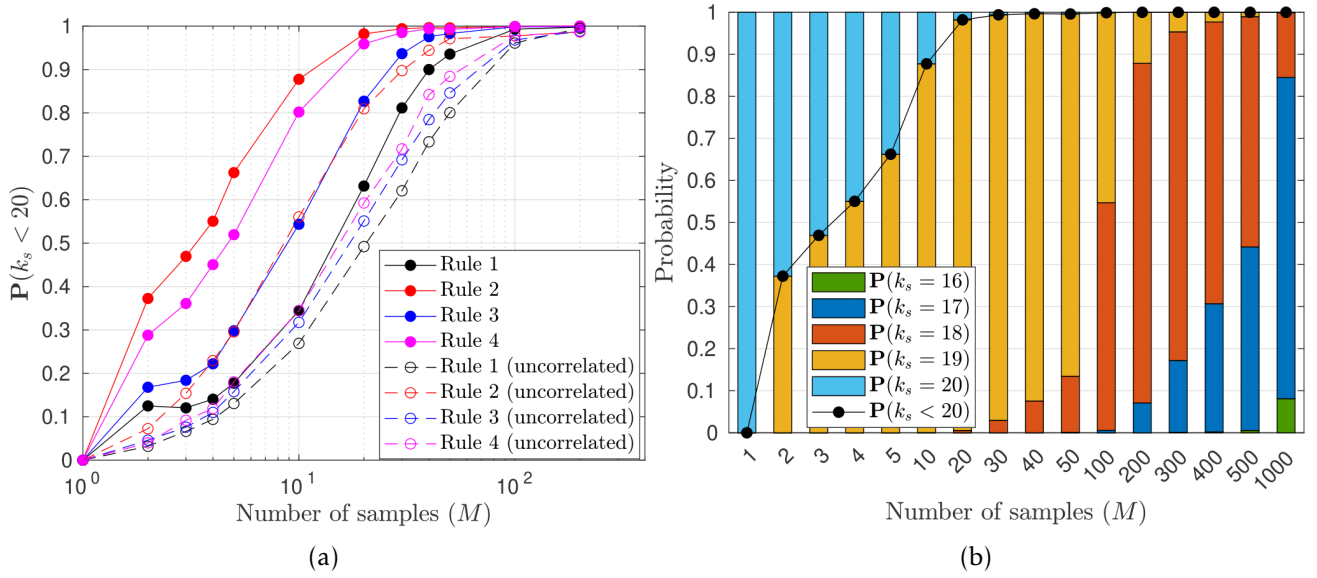


Figure 8: (a) Estimated probability that the convergence rate k_s is smaller than $k_d = 20$ as a function of M for the sampling rules with (solid lines) and without (dashed lines) correlations. Distributions were estimated by simulating 2000 independent realisations of \mathcal{P}_s for each M . (b) Estimated discrete probabilities of k_s as a function of M for sampling rule 2.

- yielding a best convergence rate $k_s = 16$ for a small proportion of runs with $M = 1000$. These results demonstrate the robustness of \mathcal{P}_s and that the sampling and propagation process is not impeded by the exponential divergence of trajectories. Additional results of \mathcal{P}_s applied to (11) are given in [Appendix D](#).

5 Conclusions

In this paper we have extended the parareal algorithm using probabilistic methods to develop a novel stochastic parareal algorithm for solving systems of ODEs in a time-parallel fashion. Instead of passing deterministically calculated initial values into parareal’s predictor-corrector, stochastic parareal selects more accurate values from a randomly sampled set, at each temporal sub-interval, to converge in fewer iterations. For the test problems in [section 4](#), we demonstrate the stochastic algorithm converges toward a solution, with accuracy of similar order to parareal, in fewer iterations than its deterministic counterpart with a given probability. Performance was measured by estimating the convergence distributions generated upon running multiple independent realisations of stochastic parareal with varying numbers of random samples M . In all test cases, the estimated probabilities of stopping sooner than parareal converge to one, given a large enough value of M is chosen.

The probabilities that stochastic parareal converges faster than standard parareal depends on a number of factors: the ODE problem being solved, the number of time sub-intervals (N) selected, the accuracy of the coarse integrator (\mathcal{G}), the number of random samples (M), and the type of sampling rule in use. By increasing the accuracy of the coarse integrator \mathcal{G} (see [Appendix A](#)), stochastic parareal was shown to perform more efficiently for problems that deterministic parareal itself struggles with. Sampling rules 1 and 3 (sampling close to the fine solutions) outperformed rules 2 and 4 (sampling close to the predictor-corrector solutions) for the ODE systems in [section 4.2](#) and [Appendix A](#). The reverse was

true, however, for the systems in [section 4.3](#) and [Appendix C](#), making it difficult to determine an optimal rule for a general ODE system. One option, to overcome having to choose a particular sampling rule, could be to sample from all four rules simultaneously during a simulation. Whilst this would require additional processors, it would yield similar performance, if not better, than using a single sampling rule. Regardless which rule is chosen, however, the expected value of the convergence rate decreases as a function of increasing M . The choice of marginal means for each sampling rule, rather than the type of distribution itself, also appeared to have more of an impact on performance. For all tested systems, generating correlated samples did, however, clearly improve performance.

Although processors are assumed to be in abundance, stochastic parareal requires at least N for its first iteration and at most $M(N - 2) + 1$ in subsequent iterations in order to achieve parallel speed-up - many more than the N required by deterministic parareal. Minimising M by optimising the sampling method is crucial when processors are limited, and it is something worth investigating. Regardless of the value of M , the stochastic iterations are designed such that they have comparable runtimes with iterations in the original algorithm. Assuming a negligible runtime for \mathcal{G} and communication times between processors (in addition to other serial computations such as determining correlations and locating optimal initial values), wallclock speed-up can be achieved by stochastic parareal.

In a small proportion of simulations (in [Appendix C](#)), it was found that stochastic parareal could in fact converge in more iterations than parareal, albeit with a very low probability. This highlights that the method of selecting the most continuous trajectory through phase space from the ensemble of sampled initial values does not necessarily guarantee the best outcome. Determining whether a better method exists using ideas from Bayesian statistics and probabilistic numerics will be the subject of future work.

In summary, we have demonstrated that probabilistic methods can be used to increase the parallel efficiency of existing time-parallel algorithms. Next we need to investigate possible improvements and generalisations. For instance, determining whether the algorithm scales for larger systems of equations - essential if it is to be used for solving PDE problems. Also, whether we can design sampling rules that do not need to be specified *a priori* - i.e. using a Bayesian framework to automatically update probability distributions at each iteration.

Acknowledgements

This work has partly been carried out within the framework of the EUROfusion Consortium and has received funding from the Euratom research and training programme 2014-2018 and 2019-2020 under grant agreement No 633053. The views and opinions expressed herein do not necessarily reflect those of the European Commission. KP is funded by the Engineering and Physical Sciences Research Council and the Medical Research Council through the MathSys II CDT (grant EP/S022244/1) as well as the Culham Centre for Fusion Energy. The authors would also like to acknowledge the University of Warwick Scientific Computing Research Technology Platform for assistance in the research described in this paper.

References

- [1] A. Toselli and O. Widlund. *Domain Decomposition Methods — Algorithms and Theory*. Springer New York, 2005.

- [2] D. Samaddar, D. P. Coster, X. Bonnin, L. A. Berry, W. R. Elwasif, and D. B. Batchelor. Application of the parareal algorithm to simulations of ELMs in ITER plasma. *Comput. Phys. Commun.*, 235:246–257, 2019.
- [3] K. Burrage. *Parallel and sequential methods for ordinary differential equations*. The Clarendon Press Oxford University Press, Burlington, MA, USA, 1995.
- [4] M. J. Gander. 50 Years of Time Parallel Time Integration. In *Multiple Shooting and Time Domain Decomposition Methods*, pages 69–113. Springer International Publishing, 2015.
- [5] B. W. Ong and J. B. Schroder. Applications of time parallelization. *Comput. Vis. Sci.*, 23:1–11, 2020.
- [6] A. Bellen and M. Zennaro. Parallel algorithms for initial-value problems for difference and differential equations. *J. Comput. Appl. Math.*, 25:341–350, 1989.
- [7] P. Chartier and B. Philippe. A parallel shooting technique for solving dissipative ODE’s. *Computing*, 51:209–236, 1993.
- [8] J. L. Lions, Y. Maday, and G. Turinici. Résolution d’EDP par un schéma en temps pararéel. *C. R. Math. Acad. Sci. Paris - Series I: Math.*, 332:661–668, 2001.
- [9] J. Nievergelt. Parallel methods for integrating ordinary differential equations. *Communications of the ACM*, 7:731–733, 1964.
- [10] P. Saha, J. Stadel, and S. Tremaine. A Parallel Integration Method for Solar System Dynamics. *The Astronomical Journal*, 114:409, 1997.
- [11] L. Baffico, S. Bernard, Y. Maday, G. Turinici, and G. Zérah. Parallel-in-time molecular-dynamics simulations. *Phys. Rev. E*, 66:4, 2002.
- [12] P. F. Fischer, F. Hecht, and Y. Maday. A parareal in time semi-implicit approximation of the navier-stokes equations. *Lect. Notes Comput. Sci. Eng.*, 40:433–440, 2005.
- [13] I. Garrido, M. S. Espedal, and G. E. Fladmark. A convergent algorithm for time parallelization applied to reservoir simulation. *Lect. Notes Comput. Sci. Eng.*, 40:469–476, 2005.
- [14] J. M.F. Trindade and J. C.F. Pereira. Parallel-in-time simulation of two-dimensional, unsteady, incompressible laminar flows. *Numerical Heat Transfer, Part B: Fundamentals*, 50:25–40, 2006.
- [15] S. Engblom. Parallel in time simulation of multiscale stochastic chemical kinetics. *Multiscale Model. Simul.*, 8:46–68, 2009.
- [16] F. Legoll, T. Lelièvre, K. Myerscough, and G. Samaey. Parareal computation of stochastic differential equations with time-scale separation: a numerical convergence study. *Comput. Vis. Sci.*, 23:1–18, 2020.
- [17] D. Samaddar, D. E. Newman, and R. Sánchez. Parallelization in time of numerical simulations of fully-developed plasma turbulence using the parareal algorithm. *J. Comput. Phys.*, 229:6558–6573, 2010.
- [18] G. Bal. On the convergence and the stability of the parareal algorithm to solve partial differential equations. *Lect. Notes Comput. Sci. Eng.*, 40:425–432, 2005.

- [19] G. Bal and Y. Maday. A “Parareal” Time Discretization for Non-Linear PDE’s with Application to the Pricing of an American Put. In *Recent Developments in Domain Decomposition Methods*, pages 189–202. Springer, Berlin, Heidelberg, 2002.
- [20] M. J. Gander and S. Vandewalle. Analysis of the parareal time-parallel time-integration method. *SIAM J. Sci. Comput.*, 29:556–578, 2007.
- [21] Y. Maday and G. Turinici. A parareal in time procedure for the control of partial differential equations. *C. R. Math. Acad. Sci. Paris*, 335:387–392, 2002.
- [22] Y. Maday and G. Turinici. The parareal in time iterative solver: A further direction to parallel implementation. *Lect. Notes Comput. Sci. Eng.*, 40:441–448, 2005.
- [23] W. R. Elwasif, S. S. Foley, D. E. Bernholdt, L. A. Berry, D. Samaddar, D. E. Newman, and R. Sanchez. A dependency-driven formulation of parareal: Parallel-in-time solution of PDEs as a many-task application. In *MTAGS’11 - Proceedings of the 2011 ACM International Workshop on Many Task Computing on Grids and Supercomputers, Co-located with SC’11*, pages 15–24, New York, New York, USA, 2011. ACM Press.
- [24] Y. Maday and O. Mula. An adaptive parareal algorithm. *J. Comput. Appl. Math.*, 377:112915, 2020.
- [25] M. J. Gander and E. Hairer. Nonlinear convergence analysis for the parareal algorithm. *Lect. Notes Comput. Sci. Eng.*, 60:45–56, 2008.
- [26] R. B. Nelsen. *An Introduction to Copulas*. Springer New York, 2006.
- [27] A Sklar. Fonctions de Répartition à n Dimensions et Leurs Marges. *Publications de L’Institut de Statistique de L’Université de Paris*, 8:229–231, 1959.
- [28] R. Lefever and G. Nicolis. Chemical instabilities and sustained oscillations. *J. Theoret. Biol.*, 30:267–284, 1971.
- [29] L.N. Trefethen, A. Birkisson, and T. Driscoll. *Exploring ODEs*. SIAM, Philadelphia, USA, 2017.
- [30] E. N. Lorenz. Deterministic Nonperiodic Flow. *J. Atmos. Sci.*, 20:130–141, 1963.

Appendix

In the following sections we illustrate some additional results using stochastic parareal.

A One-dimensional Bernoulli equation

Consider the nonlinear non-autonomous Bernoulli equation

$$\frac{du_1}{dt} = \frac{2}{1+t}u_1 - t^2u_1^2, \quad (12)$$

with initial value $u_1(0) = 2$ on $t \in [0, 10]$. We discretise using $N = 20$ sub-intervals and time steps $\delta T = 10/20$ and $\delta t = 10/2000$. Equation (12) permits the analytical solution $u_1(t) = (1+t)^2/(t^5/5+t^4/2+t^3/3+1/2)$, tending to zero as $t \rightarrow \infty$. Observe the spacing between equidistant time steps of the true \mathcal{F} solution and the \mathcal{P}_s solution to (12) in Figure 9a, demonstrating the stiffness of the solution at early times. Given the stopping tolerance $\varepsilon = 10^{-10}$, observe in Figure 9b how \mathcal{P} converges in $k_d = 8$ iterations deterministically whilst \mathcal{P}_s converges in $k_s \in \{5, 6\}$ iterations for each of the ten independent realisations shown.

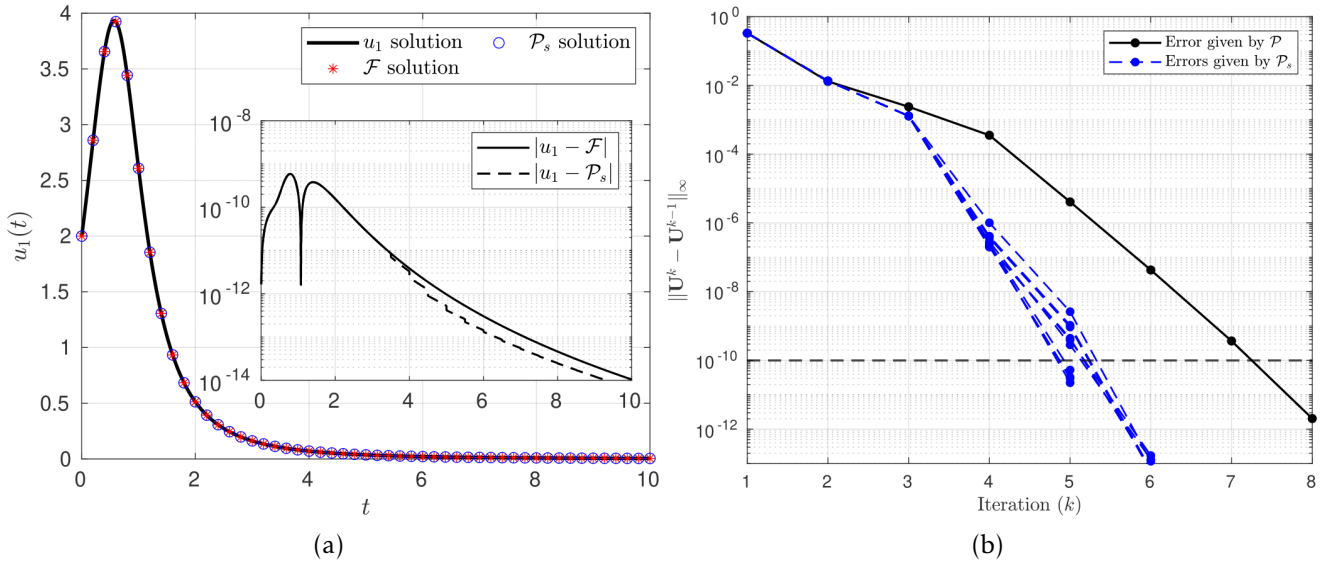


Figure 9: (a) Analytical solution u_1 of (12) plotted against numerical solutions obtained using \mathcal{F} serially and \mathcal{P}_s . Note that only a subset of the fine time steps of the numerical solutions are shown for clarity. Inset: displays the numerical errors of \mathcal{F} and \mathcal{P}_s compared to u_1 . (b) Errors at successive iterations of \mathcal{P} (black lines) and ten independent realisations of \mathcal{P}_s (blue lines). The horizontal dashed black line represents the tolerance $\varepsilon = 10^{-10}$. Both panels use \mathcal{P}_s with sampling rule 3 and (a) $M = 30$ and (b) $M = 1000$.

Figure 10a shows the estimated distributions of k_s using sampling rule 1. As expected, if $M = 1$, convergence is deterministic (i.e. $\mathcal{P}_s = \mathcal{P}$) and hence $\mathbb{P}(k_s = 8) = 1$. As M increases however, $\mathbb{P}(k_s = 8)$ decreases rapidly to zero whilst $\mathbb{P}(k_s < 8)$ increases from zero to one. This demonstrates that \mathcal{P}_s requires very few samples to begin converging in fewer iterations than \mathcal{P} , and that k_s assumes low values with increasing probabilities for increasing M . The stiffness of (12) appears to demand much larger values of M to continually reduce k_s however.

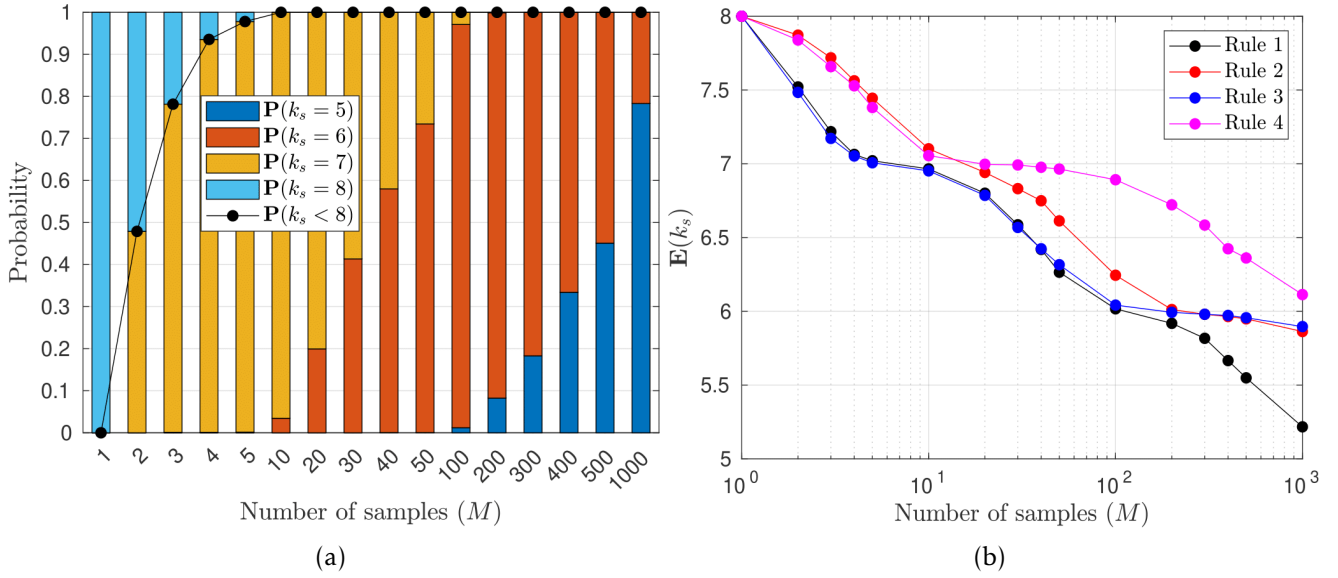


Figure 10: (a) Estimated discrete distributions of k_s as a function of M for sampling rule 1. (b) Estimated expectation of k_s as a function of M , calculated using estimated distributions of k_s for each sampling rule. Distributions were estimated by simulating 2000 independent realisations of \mathcal{P}_s for each M .

In Figure 10b we report the expected values of k_s for each sampling rule. This shows that for low values of M , using either a Gaussian or t -copula sampling rule makes little difference to performance. More interestingly, rules 1 and 3, centred around the fine solutions, outperform rules 2 and 4, which are centred around the predictor-corrector. Further testing revealed that varying the fine time steps within \mathcal{P}_s had little impact on these probabilities. On the contrary, Figure 11 shows how increasing the number of coarse steps in the interval $[0, 10]$ from 20 to 60 drastically decreases the probabilities of \mathcal{P}_s converging sooner than \mathcal{P} . Increasing the number of coarse steps increases the accuracy of the \mathcal{G} solver, hence \mathcal{P} reaches the stopping tolerance in fewer iterations k_d . This result suggests that whilst \mathcal{P}_s can still converge faster than \mathcal{P} by using more samples, it works more efficiently for particular problems where k_d is relatively large (i.e when \mathcal{P} obtains low rates of parallel speed up).

Finally, absolute errors between 250 independent \mathcal{P}_s solutions with respect to the \mathcal{F} solution (Figure 12a) and the analytical solution u_1 (Figure 12b) were determined. In both cases, we observe how the median solution attains comparable accuracy to \mathcal{P} and both the fine and analytical solutions respectively. The standard deviation between all 250 realisations is $\mathcal{O}(10^{-11})$ and the results also demonstrate that solutions which take an extra iteration to converge, i.e. $k_s = 7$ instead of $k_s = 6$, have significantly improved errors.

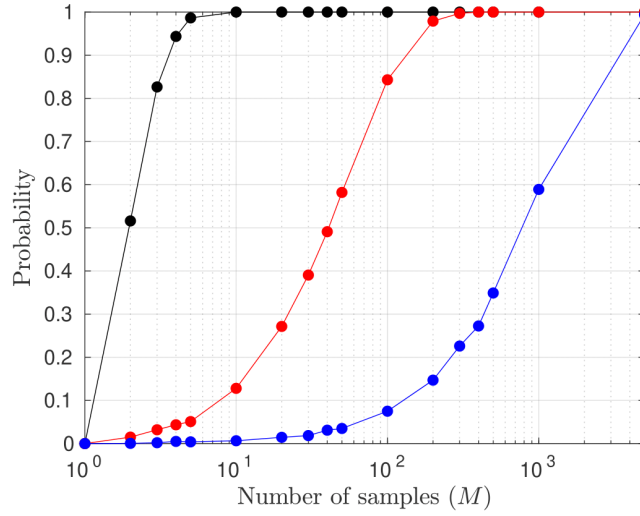


Figure 11: Estimated probabilities that the convergence rate k_s is smaller than k_d as a function of M using sampling rule 3. Each curve shows $\mathbb{P}(k_s < 8)$ (black), $\mathbb{P}(k_s < 5)$ (red), and $\mathbb{P}(k_s < 4)$ (blue) using coarse steps $\delta T = 10/20, 10/40, 10/60$ respectively - noting that \mathcal{P} converges in $k_d = 8, 5, 4$ iterations for these coarse steps respectively. As before, 2000 independent realisations of \mathcal{P}_s were run for each M .

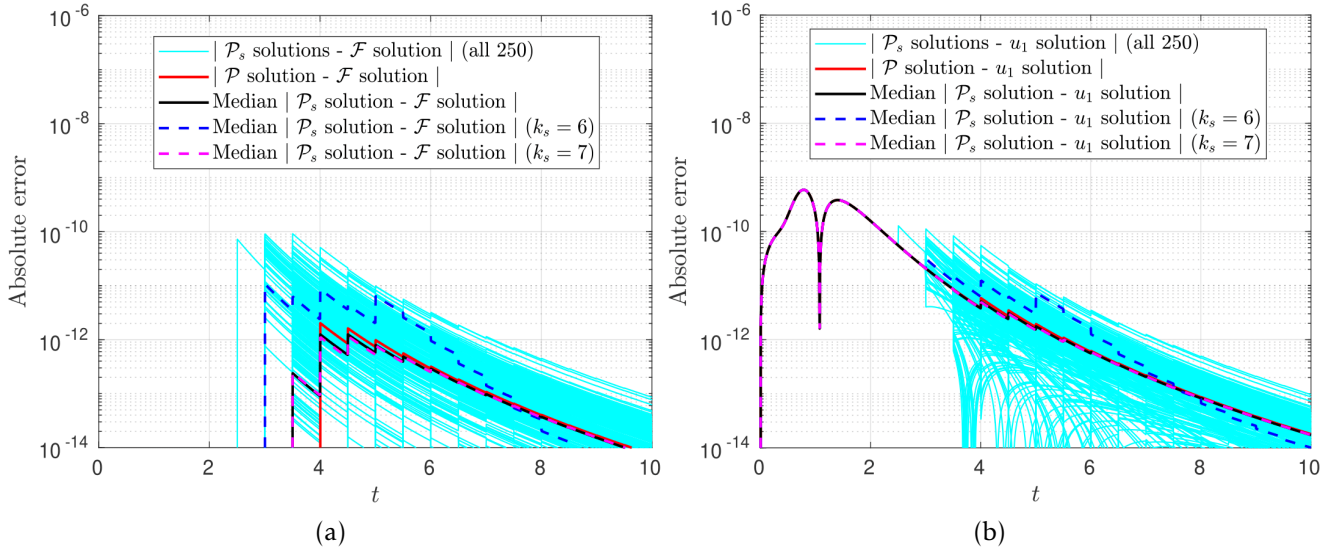


Figure 12: Absolute errors of \mathcal{P} and \mathcal{P}_s calculated against (a) the \mathcal{F} solution and (b) the analytical solution u_1 . The errors obtained from 250 independent realisations of \mathcal{P}_s using sampling rule 1 with $M = 10$ are shown in light blue. The deterministic error generated by \mathcal{P} is shown in red, the median error across all 250 simulations of \mathcal{P}_s in black, the median $k_s = 6$ error for \mathcal{P}_s in dashed blue, and the median $k_s = 7$ error for \mathcal{P}_s in dashed purple.

B Two-dimensional Brusselator system

The additional results here complement subsection 4.2. The numerical solutions to system (4.2) in the phase plane are given in Figure 13a alongside the errors at successive iterations of five runs of \mathcal{P}_s in Figure 13b. In Figure 14 we report the expected value of k_s as a function of M for each of the sampling rules. This result suggests that larger values of M are required to reduce $\mathbb{E}(k_s)$ even further for this stiff system. In Figure 15, the numerical errors of each solution component (u_1 and u_2) are plotted against the \mathcal{F} solution. Observe again how the median \mathcal{P}_s solutions attain an equivalent, or better, accuracy than the that generated by \mathcal{P} .

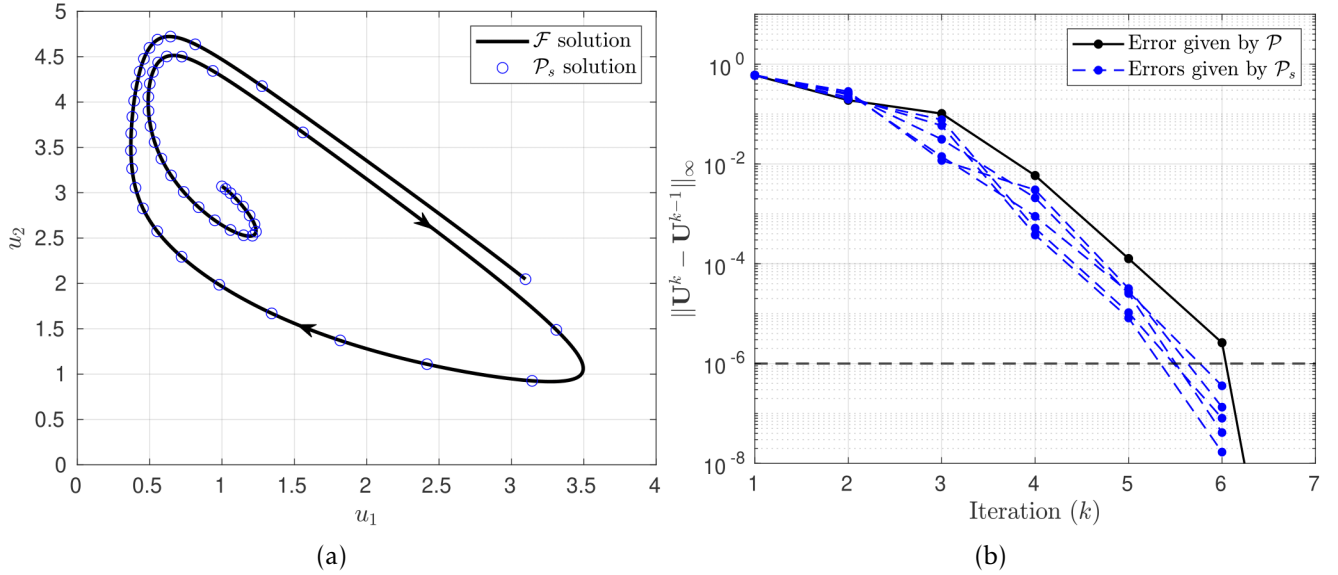


Figure 13: (a) Numerical solution of system (4.2) in the phase plane using \mathcal{F} and \mathcal{P}_s . Note again, not all fine points of \mathcal{P}_s solution are shown for clarity. (b) Errors at successive iterations of \mathcal{P} (black lines) and five independent realisations of \mathcal{P}_s (blue lines). Horizontal dashed black line represents the tolerance $\varepsilon = 10^{-6}$. Both panels run \mathcal{P}_s with sampling rule 1 and $M = 10$.

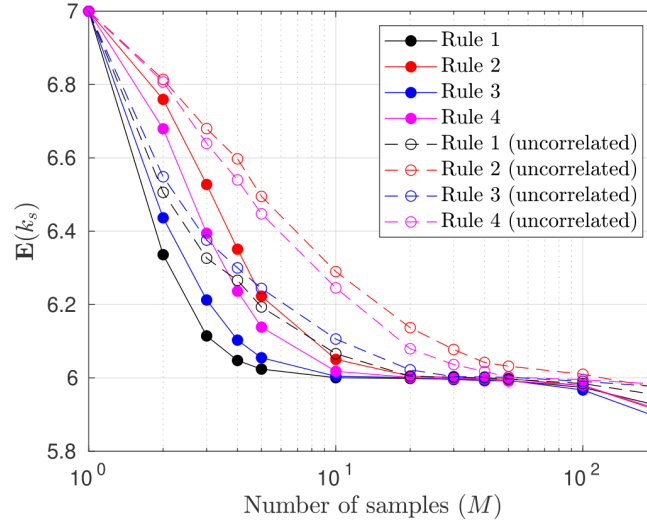


Figure 14: Estimated expectation of k_s as a function of M , calculated using estimated distributions of k_s for each sampling rule with (solid lines) and without (dashed lines) correlations. Distributions are estimated by simulating 2000 independent realisations of \mathcal{P}_s for each M .

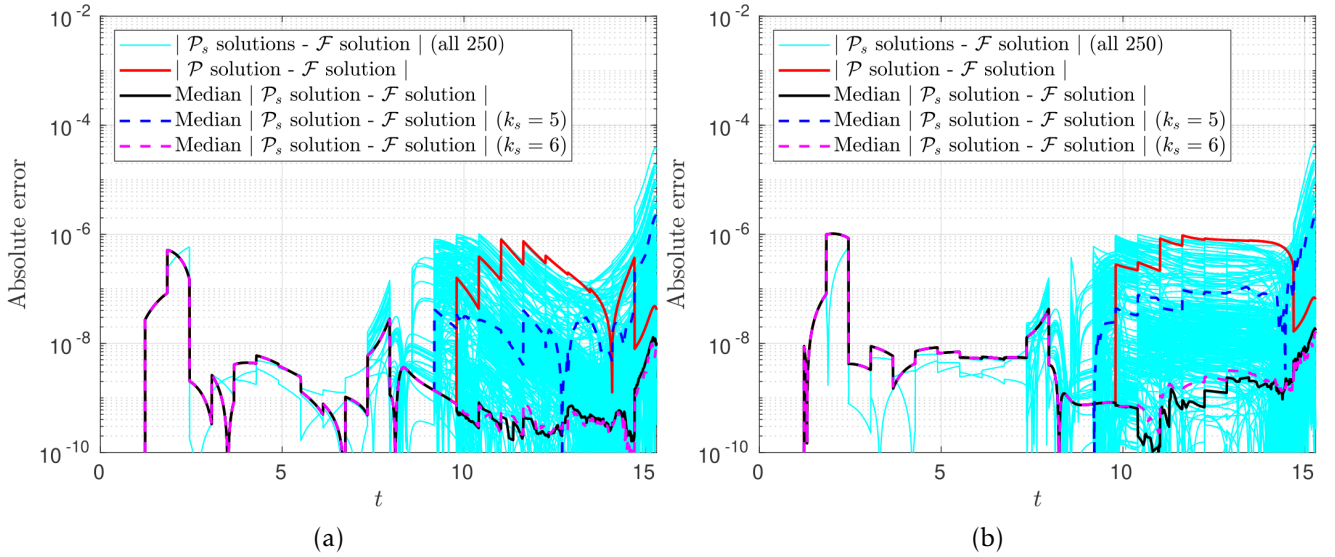


Figure 15: Absolute errors of \mathcal{P} and \mathcal{P}_s calculated against the \mathcal{F} solution. The errors obtained from 250 independent realisations of \mathcal{P}_s using sampling rule 4 with $M = 200$ are shown in light blue. The deterministic error generated by \mathcal{P} is shown in red, the median error across all 250 simulations of \mathcal{P}_s in black, the median $k_s = 5$ error for \mathcal{P}_s in dashed blue, and the median $k_s = 6$ error for \mathcal{P}_s in dashed purple. Panel (a) displays errors for the u_1 component of the solution whilst (b) displays the u_2 component.

C Two-dimensional ‘square limit cycle’ system

Consider the system

$$\frac{du_1}{dt} = -\sin(u_1) \left(\frac{\cos(u_1)}{10} + \cos(u_2) \right), \quad (13a)$$

$$\frac{du_2}{dt} = -\sin(u_2) \left(\frac{\cos(u_2)}{10} - \cos(u_1) \right), \quad (13b)$$

whose solutions, for initial values within the box $[0, \pi] \times [0, \pi]$, converge toward a square-shaped limit cycle on the edges of the box (see Figure 16a) [?]. The system is solved on $t \in [0, 60]$, starting at $\mathbf{u}(0) = (3/2, 3/2)^T$, using $N = 30$ sub-intervals and time steps $\delta T = 60/30$ and $\delta t = 60/3000$. As shown in Figure 16b, \mathcal{P} takes $k_d = 20$ iterations to converge with tolerance $\varepsilon = 10^{-8}$ whilst the ten realisations of \mathcal{P}_s shown take between $17 \leq k_s \leq 19$.

Contrary to the previous two-dimensional test problem, Figure 17a shows that sampling close to the predictor-corrector values (rules 2 and 4) yield lower expected values of k_s . In this case, the bivariate Gaussian outperforms the t -copula, however the reverse is true for rules 1 and 3. Results using uncorrelated samples have been shown to generate inferior performance hence are not shown here. The detailed distributions of k_s in Figure 17b, using sampling rule 2, show a best performance of $k_s = 14$ with 100 samples. They do, however, reveal that in a limited number of cases, using 2 or 3 samples, \mathcal{P}_s can in fact take more than $k_d = 20$ iterations to converge. This suggests that the way the optimal trajectory is chosen does not bound k_s above by k_d in a small minority of realisations - something to be investigated in future work.

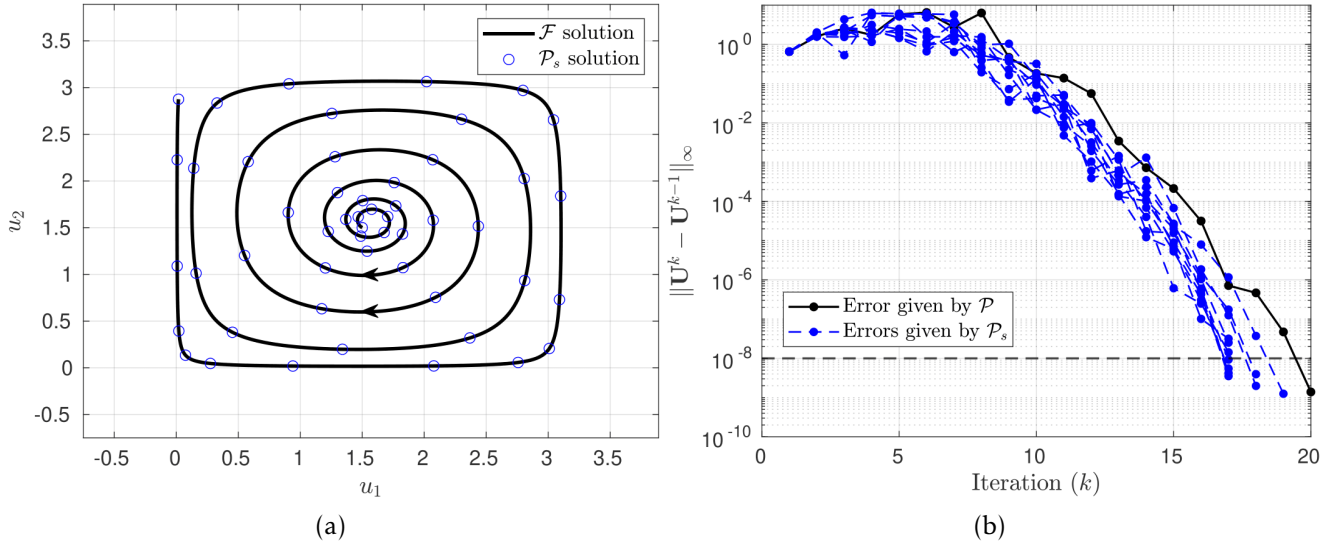


Figure 16: (a) Numerical solution of (13) over $[0, 60]$ using \mathcal{F} serially and \mathcal{P}_s . Note again that only a subset of the fine time steps of the \mathcal{P}_s solution are shown for clarity. (b) Errors at successive iterations of \mathcal{P} and ten independent realisations of \mathcal{P}_s . Dashed black line represents the tolerance $\varepsilon = 10^{-8}$. Note that both panels use \mathcal{P}_s with sampling rule 2 and $M = 20$.

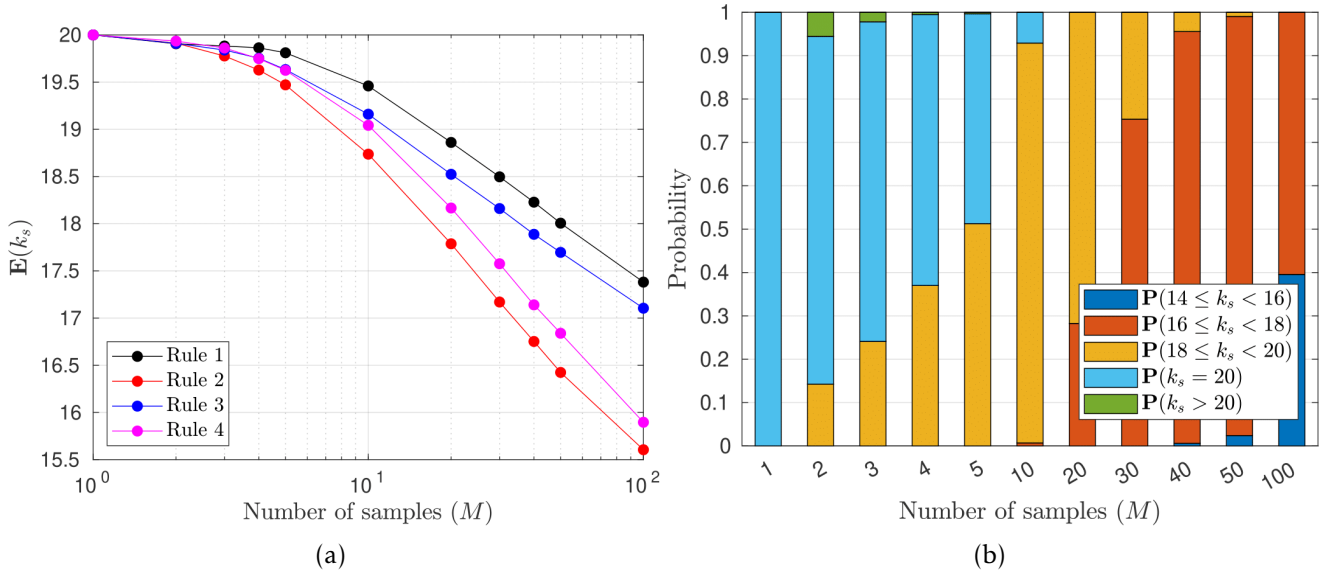


Figure 17: (a) Estimated expectation of k_s as a function of M , calculated using estimated distributions of k_s for each sampling rule. (b) Estimated discrete distributions of k_s as a function of M for sampling rule 2. Distributions were calculated by simulating 2000 independent realisations of \mathcal{P}_s for each M .

D Three-dimensional Lorenz system

The additional results here complement subsection 4.3. Figure 18 displays $\mathbb{E}(k_s)$ against M , indicating that for the Lorenz system, generating correlated samples close to the predictor-corrector solutions (sampling rules 2 and 4) yield the lowest expected values of k_s .

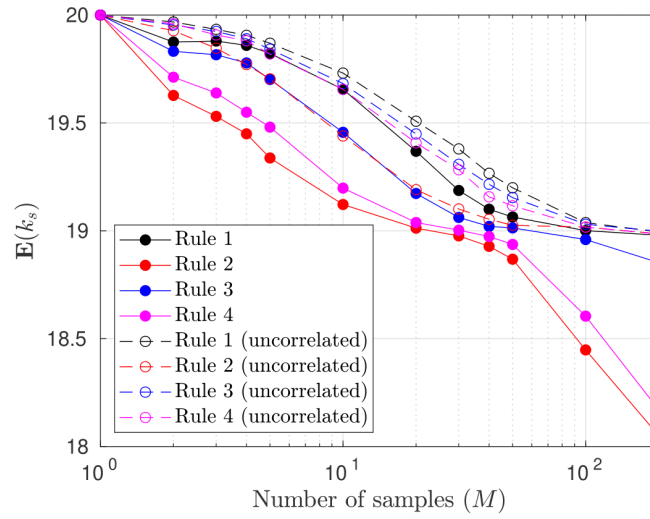


Figure 18: Estimated expectation of k_s as a function of M , calculated using estimated distributions of k_s for each sampling rule with (solid lines) and without (dashed lines) correlations. Distributions are estimated by simulating 2000 independent realisations of \mathcal{P}_s for each M .